Available online at www.sciencedirect.com
SCIENCE DIRECT®
International Journal of Heat and Fluid Flow 24 (2003) 157–180
International Journal of HEAT AND FLUID FLOW
www.elsevier.com/locate/ijhff

Investigation of wall-function approximations and subgrid-scale models in large eddy simulation of separated flow in a channel with streamwise periodic constrictions

Lionel Temmerman [a], Michael A. Leschziner [a,*], Christopher P. Mellen [b], Jochen Fröhlich [b]

[a] *Department of Aeronautics, Imperial College of Science, Technology & Medicine, Prince Consort Road, London SW7 2BY, UK*
[b] *Institute for Hydromechanics, University of Karlsruhe, Kaiserstrasse 12, 76128 Karlsruhe, Germany*

Received 12 October 2001; accepted 12 September 2002

Abstract

Large eddy simulations are presented for the flow in a periodic channel segment, which is laterally constricted by hill-shaped obstructions on one wall, having a height of 33% of the unconstricted channel. The Reynolds number, based on channel height, is 21,560. Massive separation thus arises on the hills' leeward sides, the length of which is about 50% of that of the periodic segment. After reattachment, the flow is allowed to recover over about 30% of the segment length before being strongly accelerated over the windward side of the next hill. The principal challenge of this flow arises from the separation on the curved hill surface and the fact that the reattachment point, and hence the whole flow, are highly sensitive to the separation process. Simulations were performed with three grids, six subgrid-scale models and eight practices of approximating the near-wall region in simulations on the two coarser grids. These were supported by wall-resolved and wall-function simulations for fully-developed channel flow. The principal objective is to identify the sensitivity of the predictive accuracy to resolution and modelling issues. Coarse-grid simulations are judged by reference to data derived from two independent highly-resolved simulations obtained over identical meshes of close to 5 million nodes. Similarly, coarser-grid simulations were also performed with the two codes to enhance confidence in the results. The principal message emerging from the simulations is that grid resolution, especially in the streamwise direction around the mean separation position, has a very strong influence on the reattachment behaviour and hence the whole flow. This has serious implications for even more challenging high-Reynolds-number cases in which separation occurs from gently curved surfaces. The near-wall treatment, including the details of the numerical implementation of the wall laws, is also shown to be influential, most prominently on the coarsest grid. The application of the no-slip conditions at the wall at which separation occurs is found to cause substantial errors, especially in conjunction with poor streamwise resolution, even if the wall-nearest grid nodes are within the semi-viscous sublayer, in the range $5 \lesssim y^+ \lesssim 15$. The sensitivity to subgrid-scale modelling is shown to be more modest, with those models returning relatively low subgrid-scale viscosity giving the closest accord with the highly-resolved simulation.
© 2002 Elsevier Science Inc. All rights reserved.

Keywords: Large eddy simulation; Wall functions; Separated flow; Constricted channel; Wavy wall; Subgrid-scale models

1. Introduction

Numerous studies undertaken over the past few years (Lesieur and Métais, 1996; Moin, 1998; Germano, 1998; Meinke and Krause, 1998) demonstrate that LES returns impressive predictive accuracy in flows which feature pronounced periodic components and/or in which turbulence transport is dictated by the dynamics of the large-scale eddies associated with separated shear layers. Examples are vortex shedding behind bluff bodies in a free stream (Rodi, 1998; di Mare and Jones, 1999), or behind wall-mounted bluff obstacles (Thomas and Williams, 1999) or jets in crossflow (Jones and Wille, 1996a,b). In all of these cases, the viscous influence of the walls, if present, is weak and the spatial scales are

* Corresponding author. Tel.: +44-20-75945061; fax: +44-20-75848120.
E-mail address: mike.leschziner@ic.ac.uk (M.A. Leschziner).

0142-727X/03/$ - see front matter © 2002 Elsevier Science Inc. All rights reserved.
doi:10.1016/S0142-727X(02)00222-9

such that they can be resolved reasonably well by a relatively coarse, low-aspect-ratio (i.e. close-to-isotropic) grid with the internodal distance being of order 1% of the scale of the whole flow. In such circumstances, the non-dissipative processes taking place at subgrid-scale level are not influential. Moreover, the numerical errors associated with the resolution of the influential scales are relatively low, even with second-order schemes, because these scales have large wavelength-to-grid-distance ratios and therefore appear relatively smooth to the grid.

There are many practically important flows and flow conditions which do not fall into the above 'benign' category and which present LES with a much greater challenge. These are, almost invariably, of a type in which the viscous near-wall processes have a major direct or indirect influence on the primary flow properties. It might be supposed, for example, that a fully-developed channel flow would be easily resolved well by a standard LES method. However, this is not generally the case at high Reynolds numbers, unless an extremely fine grid is used, which resolves the viscous sublayer down to a wall-normal distance $y^+ = \mathrm{O}(1)$, whilst also providing a streamwise and spanwise resolution $(\Delta x^+, \Delta z^+) = \mathrm{O}(50, 10)$. In effect, the LES is required to approach, without further modelling, a DNS near the wall, where the dynamically important scales diminish rapidly towards the dissipative ones, and turbulence approaches a two-component state. An under-resolved LES tends to return, among others, an erroneous log-law and excessive anisotropy. Errors can be substantially compounded by numerically disadvantageous features, such as high rates of grid expansion or contraction, insufficient box size and low order of approximation. The simulated channel flow is also materially sensitive to subgrid-scale modelling, especially the asymptotic behaviour of the subgrid-scale viscosity at the wall.

The difficulties highlighted above are pertinent to a whole range of flows in which the adequate resolution of boundary layers is an essential pre-requisite to the correct representation of gross flow features that are sensitive to the structure of the boundary layers. Probably the most important group includes flows in which a boundary layer separates from a gently curved or sloping wall due to the geometry-induced adverse pressure gradient. This occurs, for example, on a highly-loaded aerofoil or blade, in a diffuser, in a curved duct, in a channel constricted by a stenosis and on wavy terrain at sufficiently high undulation amplitude. In all these cases, the structure of the boundary layer will influence the separation line, both instantaneous and time-averaged. At the high Reynolds numbers encountered in practical applications, the resource requirements of a wall-resolving simulation quickly become prohibitive, because of the need to resolve the thin (possibly transitional) boundary layer as well as the details of the extensive region within which the separation line moves in time and the large-scale structures within the separated shear layer and the recirculation zone. In the case of a spanwise homogeneous flow—for example, an infinitely-swept wing or a very wide duct—the largest scales dictate the spanwise extent of the simulation box, the typical ratio of the two being 1:4. To resolve the streaky spanwise structure of the boundary layer within such a box may require hundreds of spanwise grid planes and tens of millions of nodes. This is untenable in most circumstances, and a compromise must be struck between resolution and economy to allow the simulation of such flows. Thus, Kaltenbach and Choi (1995) and Jansen (1996), both simulating the separated flow around the NACA 4412 aerofoil at $Re = 1.64 \times 10^6$, restricted the spanwise extent to a maximum of 5% of chord, yet used a mesh of 2.4×10^6 nodes with a mere 48 spanwise grid planes. Another example is the simulation of Kaltenbach et al. (1999) of a separated flow at the moderate Reynolds number of 30,000 within an asymmetric plane diffuser. In this, the spanwise direction was treated as statistically homogenous, with the spanwise-distance-to-channel-height ratio reducing from 4 upstream of the diffuser to only 1.5 downstream where the largest structures are encountered.

Near-wall resolution is also of concern in simulations of separated flow over a wavy wall, a configuration of particular interest in the context of meteorological issues. LES studies by Henn and Sykes (1999), Armenio and Piomelli (2000) and Salvetti et al. (2001) examine flows over sinusoidally undulating walls at various amplitude-to-wavelength ratios ("wave-slope") and channel-height values of 5–10 wave amplitudes. When the wave slope exceeds about 0.05, separation occurs in the trough, although this is often small and longitudinally inhibited by the pitch. Only the study by Salvetti et al. (2001) can be regarded as addressing a high Reynolds-number flow, in so far as near-wall resolution becomes a serious problem. In that study—as in all others on wavy-wall flows—a no-slip (NS) condition was prescribed at the wall, even when the first computational node was, in Salvetti et al's case, as far away from the wall as $y^+ = 150$. None of the studies addressed the sensitivity of the simulation to variations in the near-wall treatment and, in any breadth, to subgrid-scale modelling, while resolution issues were considered, at most, by reference to two meshes, and then at relatively low Reynolds numbers (based on wave amplitude).

In an effort to achieve a substantial reduction in the resource requirements of LES for high Reynolds-number near-wall flows, yet maintain a realistic description of the effects of near-wall processes on the outer flow, a number of alternative approximations of the semi-viscous near-wall layer have been explored since the first computations of Deardorff (1970) and continue to be of considerable interest today due to their practical rele-

vance. Several approaches have emerged, one of which is to adopt an assumed shape for the instantaneous velocity between the nodes closest to the wall and the wall itself. Variants of this "wall-function" approach arise from the use of the 1/7th power-law profile (Werner and Wengle, 1991) and the log-law profile (Grötzbach, 1987). Both are designed to return an estimate of the instantaneous wall shear stress for a given velocity at the wall-nearest node, which then serves as a wall boundary condition. An alternative method by Schumann (1975) estimates the instantaneous wall-shear stress from the instantaneous near-wall velocity and the ratio of the *time-averaged* values of the two, the latter obtained from the time-mean law of the wall and the time-averaged near-wall velocity. As is shown by Wille (1997) and also later in this paper, wall-function methods allow reasonable simulations of channel flow to be achieved on rather coarse grids. Virtually nothing is known, however, about the effectiveness of the technique in separated flows.

Another route involves the use of unsteady RANS methods, employing conventional turbulence models, for the near-wall layer. This layer is then matched to the outer LES region, either at a prescribed interface or a location dictated by a length-scale criterion. The RANS scheme may involve the solution of the full Navier–Stokes equations, or their thin shear-layer forms or even algebraic simplifications thereof, which approximate the transport terms using the interface values or ignore them altogether. The underlying rationale is that RANS solutions for attached near-wall flow are relatively insensitive (at least in statistically steady conditions) to the streamwise and spanwise resolution, provided the wall-normal grid is fine enough. This is in contrast to the low-aspect-ratio (i.e. very expensive) grids required for adequate simulations of the near-wall layer. One variant of this two-layer method is that of Balaras et al. (1996) and Hoffmann and Benocci (1994) who used a mixing-length model to determine the eddy viscosity in the sublayer. A recent study by Cabot and Moin (1999) demonstrates that this approach yields acceptable results for channel and backward-facing-step flows. Another variant is that of Spalart et al. (1997) in which the eddy viscosity is obtained from the Spalart-Almaras one-equation model. This particular combination, referred to as detached eddy simulation (DES) was applied by Shur et al. (1999) to a high-incidence aerofoil in which the flow separated close to the aerofoil's leading edge. This cannot be regarded as a searching test case, however, because separation is induced in a region of intense curvature, so that the location of the separation line is not materially sensitive to the structure of the upstream boundary layer. The DES method was later applied to the attached flow in a turbulent plane channel by Nikitin et al. (2000) with moderate success. While intended to be used with a substantially coarser discretisation in the streamwise and spanwise directions, relative to conventional LES, the method was observed to generate an artificial buffer layer around the plane interfacing the near-wall and LES regions. As the Reynolds number increases, DES relies on a progressive rise in wall-normal grid density, to ensure an appropriate resolution of the viscous near-wall region. This has two major consequences: first, resource implications become increasingly important; second, extremely high cell aspect ratios occur near the wall. The latter might be acceptable in steady RANS computations, but with LES, the level of unsteadiness and its contribution to the statistics remain high. Hence, the large aspect ratio may have a seriously deleterious effect on accuracy in flows in which viscous near-wall processes are important.

A different hybrid strategy, involving the use of a two-equation k–ω model for the near-wall layer, was recently applied by Davidson and Peng (2001) to a channel flow and the separated hill-in-channel flow, which is also the primary focus of this paper. The results were variable, featuring an anomalous behaviour in the interface region and demonstrating the challenges of matching properly the RANS layer to the LES region.

In an earlier paper, Davidson (2000) also reports rather poor DES computations for that same separated hill-in-channel flow, but the observed errors may have been caused, at least in part, by the excessively coarse 170,000-node grid used. There is no doubt that much research remains to be done before the pros and cons of DES and other LES-RANS hybrid methodologies are fully understood in the context of simulating high-Reynolds-number near-wall flows.

In this paper—a companion to that of Mellen et al. (2002b)—we investigate the effectiveness of using different wall-function formulations within an LES methodology applied to a flow which separates from a curved surface. The geometry, shown in Fig. 1, is a periodic, spanwise-homogeneous channel segment with one wall containing hill-shaped constrictions, with a streamwise period of 9 hill heights. This geometry leans on an experimental configuration examined by Almeida et al. (1993), and it was designed to meet a number of specific desiderata judged to be associated with a good test case for LES studies. Detailed arguments justifying the choice are contained in Mellen et al. (2002b).

In the absence of experimental data for the new configuration, highly resolved simulations have been performed with two entirely independent LES codes to generate reference data, and the two sets of results agree closely. In the companion paper (Mellen et al., 2002b), these simulations are presented in detail and analyzed in terms of the fundamental physical properties of the flow, including stress budgets and spectra. The present paper focuses on the LES modelling of the flow by using substantially coarser grids, with the highly resolved simulations serving as a benchmark. In particular, the

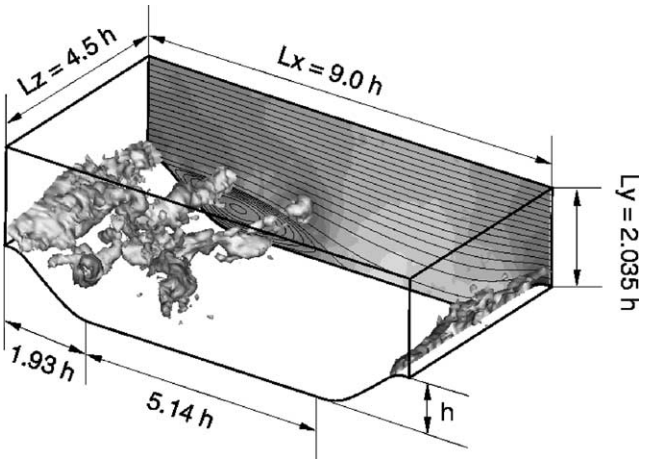

Fig. 1. Geometry of periodic-hill flow with instantaneous iso-pressure and time-averaged streamfunction contours obtained in highly-resolved LES.

sensitivity of the solution to subgrid-scale modelling, grid density and approximate near-wall treatments is investigated.

In what follows, Section 2 discusses key features of the present flow configuration. In Section 3, the subgrid-scale models employed are presented and briefly discussed. Section 4 gives information about the wall models being used, while Section 5 outlines the numerical schemes of the two codes employed. In presenting different models and implementation variants, we make use of abbreviations defined in the text and summarised in Table 1. Results are presented and discussed in Sections 7 and 8, leading to the conclusions contained in Section 9.

Table 1
List of abbreviations

Abbreviation	Signifies
BF	Backflow wall law
DES	Detached-eddy simulation
DNS	Direct numerical simulation
DSM	Dynamic Smagorinsky model
DMM	Dynamic mixed model
LDSM	Localized dynamic Smagorinsky model
LES	Large-eddy simulation
LESSOC	University of Karlsruhe Code
LL2	Two-layers log-law (point-wise)
LL2-i	Integrated form of LL2
LL3	Three-layers log-law
LLK	Two-layers log-law using the resolved turbulence energy
MSM	Mixed-scale model
NS	No-slip wall-treatment
RANS	Reynolds-averaged Navier–Stokes
SGS	Subgrid-scale
SIP	Strongly implicit procedure
SLOR	Successive line over-relaxation
SM	Smagorinsky model
SSM	Scale-similarity model
STREAMLES	Imperial College Code
WALE	Wall-adapting local eddy-viscosity model
WD	Wall-damping function ($A^+ = 25$)
WW	Werner–Wengle wall law (integrated form)
WW-p	Point-wise form of WW

2. The simulated configuration

The present configuration has been specifically defined as a test case for investigating issues of subgrid-scale and wall-modelling in the presence of massive separation from a smooth curved surface (Mellen et al., 2000). As such, the flow has to contain the key generic phenomena of interest, whilst being amenable to a simulation at economically tolerable cost.

The chosen geometry is based on the periodic configuration studied experimentally by Almeida et al. (1993). Concerns about the geometric parameters of that configuration—especially the short crest-to-crest distance typical of the wavy-terrain geometries mentioned in Section 1, about the accuracy of the experimental data and about the implied computational costs have motivated the definition of a modified geometry so as to satisfy, as well as possible, the needs and objectives of the present LES study. The rationale of the modifications is discussed in detail in Mellen et al. (2000, 2002b) by reference to several related configurations examined in past studies.

The geometry of the periodic segment is shown in Fig. 1. The shape of the constrictions has been retained from Almeida et al. (1993) and is available in the ERCOFTAC database. [1] The channel height is $L_y = 3.035$ h and the streamwise period length is $L_x = 9h$. The Reynolds number, based on the bulk velocity above the hill crest and the hill height, is $Re_h = 10595$, corresponding to $Re_{L_y} = 21{,}560$, based on the channel height and the bulk velocity. While this value is not as high as might be desirable for investigating the effectiveness of wall-functions in engineering-flow conditions, it had to be kept down to a level allowing almost fully resolved simulations to be undertaken at tolerable cost. Such simulations were undertaken with a mesh of about 5 million nodes at a cost of about 30,000 CPU hours per run on a Cray T3E. With this mesh, the ratio of internodal distance to the Kolmogorov length was of order 5–8 over most of the flow domain. At these conditions, the subgrid-scale viscosity is of the order of the fluid viscosity in the outer flow (away from the wall) and subgrid-scale transport is insignificant.

Streamwise periodicity removes the need for a specification of inflow conditions, thus eliminating a number of potential sources for error and differences between

[1] http://fluindigo.mech.surrey.ac.uk/database/

results arising from different codes. The required flow rate was imposed through a pressure-forcing term which was kept constant in space and adjusted in time so as to yield, at each instant, the desired flow rate. Thus, the bulk Reynolds number was held invariant across the entire range of simulations, while the pressure gradient varied from simulation to simulation, depending upon the wall-shear stress returned by the associated simulation.

The need for streamwise decorrelation is well understood in channel-flow simulations in which, typically, $L_x/L_y = \pi$. In the present case, decorrelation is aided by the relatively large periodic crest-to-crest distance, $L_x = 9h$. With this choice, reattachment is not enforced by the closeness of consecutive hills, in contrast to the 'wavy-terrain' configuration mentioned earlier. This renders the structure of the separation region much more sensitive to the quality of the simulation and the modelling details, which is desirable for a searching assessment. The spanwise extent is $L_z = 4.5h$, with periodicity of the instantaneous flow being imposed. Ideally, L_z would have been chosen to be even larger, as discussed in Mellen et al. (2000). Thus, although the spanwise correlation of the streamwise velocity was observed to decay to zero within half of the spanwise extent in most regions of the domain, values of around −0.2 at the half-span position prevailed in some parts of the free shear layer. However, the effect of this on the flow properties of interest were observed to be insignificant. Thus, the separation and reattachment locations resulting from a coarse-grid LES (performed on what is referred to as "Grid 1" in Fig. 2) only changed from 0.5 to 0.45 and from 3.20 to 3.25, respectively, when the spanwise domain size was doubled, with the spanwise resolution being maintained by also doubling the number of spanwise grid planes. The influence of the spanwise domain size on the flow physics is further assessed in Mellen et al. (2002b). Limiting the spanwise domain to $L_z = 4.5h$ may therefore be claimed to have introduced only a minor deviation from an infinite domain, and this value was used in all but one of the computations reported below. This choice is significantly less restrictive than that implied by the 'minimal flow unit' of Jiménez and Moin (1991).

3. Subgrid-scale modelling

3.1. Overview

The application of any spatial filtering operation to the Navier–Stokes equations—here, done implicitly through the numerical approximation being tied to the cell size Δ—leads to the LES equations:

$$\frac{\partial \overline{u}_i}{\partial t} + \frac{\partial \overline{u}_i \overline{u}_j}{\partial x_j} = -\frac{\partial \overline{p}}{\partial x_i} + 2\nu \frac{\partial \overline{S}_{ij}}{\partial x_j} - \frac{\partial \tau_{ij}}{\partial x_j} \tag{1}$$

where $\overline{S}_{ij} = 1/2\left(\partial \overline{u}_i/\partial x_j + \partial \overline{u}_j/\partial x_i\right)$ and $\tau_{ij} = \overline{u_i u_j} - \overline{u}_i \overline{u}_j$ represents the unknown subgrid-scale stresses arising from the presence of scales smaller than the filter width.

With one exception, the models used herein to approximate the subgrid-scale stresses are based on the eddy-viscosity concept,

$$\tau^a_{ij} = \tau_{ij} - \tfrac{1}{3}\delta_{ij}\tau_{kk} = -2\nu_t \overline{S}_{ij} \tag{2}$$

where ν_t is the SGS viscosity. The contribution from the diagonal term proportional to τ_{kk} is lumped into a modified pressure and does not need to be accounted for. For positive viscosity, this formulation possesses desirable (though not necessarily correct) dissipative properties, but provides—as is the case with

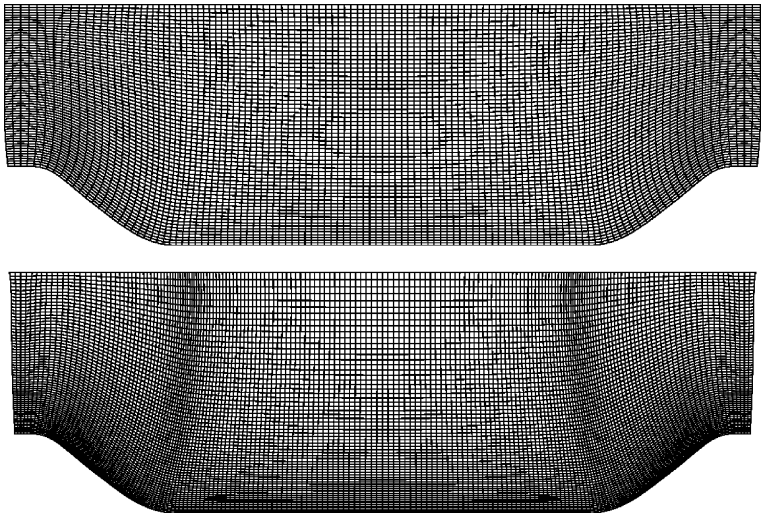

Fig. 2. Cuts in the x–y plane through the two coarse grids used to investigate approximate near-wall treatments. Above: Grid 1. Below: Grid 2.

RANS-based eddy-viscosity formulations—a poor representation of SGS transport. This latter weakness is not especially important when the SGS eddies are small, relative to the resolved range of energetic eddies which tend to strongly dominate turbulence transport, but can be seriously detrimental to accuracy when the resolved range is narrow, i.e. when the grid is (locally or globally) coarse.

The SGS models investigated in simulations to be presented are as follows:

- The constant-coefficient Smagorinsky model (SM) (Smagorinsky, 1963);
- The dynamic Smagorinsky model (DSM) (Germano et al., 1991; Lilly, 1992);
- The localized dynamic Smagorinsky model (LDSM) (Piomelli and Liu, 1995);
- The mixed-scale model (MSM) (Sagaut, 1996);
- The wall-adapted local eddy-viscosity (WALE) model (Ducros et al., 1998);
- The dynamic mixed model (DMM) (Zang et al., 1993), based on the scale-similarity model (Bardina et al., 1980);

The last model in the above list is not of the eddy-viscosity type and is able to account for backscatter. However, as discussed below, its stable implementation requires the addition of dissipation by means of an eddy-viscosity contribution, which then limits the level of backscatter the model is able to return.

3.2. Smagorinsky-type models

All models considered in this section are based on the original Smagorinsky formulation (SM) (Smagorinsky, 1963)

$$\tau_{ij}^a = -2(C_s\overline{\Delta})^2|\overline{S}|\overline{S}_{ij} = -2\nu_t\overline{S}_{ij} \tag{3}$$

where $|\overline{S}| = (2\overline{S}_{ij}\overline{S}_{ij})^{1/2}$, $\overline{\Delta} = (\Delta x\Delta y\Delta z)^{1/3}$ and $C_s = 0.1$ in the basic constant-coefficient form of (3).

One obvious defect of this basic form is that the SGS viscosity does not vanish at solid walls where the flow is, effectively, laminar. To address this defect, C_s is here multiplied by the van Driest damping function (Van Driest, 1956):

$$l = 1 - \mathrm{e}^{-y^+/A^+} \tag{4}$$

with A^+ taken as 25 (WD). While this does not give the correct (cubic) *rate* of decay (Hinze, 1975) as the wall is approached, it does ensure that the SGS viscosity vanishes within the viscous sublayer.

The dynamic form of the Smagorinsky model (DSM), Germano et al. (1991), allows for C_s to vary spatially and temporally through a process in which the evolving resolved flow is test-filtered on on a coarser scale. Here, we adopt the test filter $\widehat{\overline{\Delta}} = 2\overline{\Delta}$ together with the least-squares minimization of Lilly (1992). The resulting value of C_s varies rapidly in time and space, frequently becoming negative. For reasons of numerical stability, C_s needs to be limited and smoothed by means of temporal or spatial averaging. Thus, in all computations reported below averaging has been performed in the homogeneous directions of the flow and the positivity constraint $\nu + \nu_t \geqslant 0$ has been applied.

The LDSM is another variation of Germano's proposal, introduced by Piomelli and Liu (1995). This is intended to circumvent the difficulty that the spatially varying coefficient C_s cannot be formally extracted from the tensorial test-filter stress–strain relationship of Germano, unless it is assumed to be invariant across the test-filtered domain. This is done by retaining the spatially-varying C_s, as is formally correct, under the test-filtered subgrid-scale stress tensor and then using a spatially varying estimate C_s^* from the previous time step to approximate C_s under the test filter. Otherwise, Lilly's least-square minimisation is again applied to determine C_s. This method has been found to be fairly stable in the present study, subject to local averaging of C_s being performed with values at immediate neighbouring nodes and the constraint of positive total viscosity being imposed.

The MSM, proposed by Sagaut (1996), combines the Smagorinsky SGS viscosity, $\nu_t = (C_s\overline{\Delta})^2|\overline{S}|$, assumed to relate to the large scales, with $\nu_t = C_q\overline{\Delta}q^{1/2}$, relating to the small scales, where q is the SGS turbulence energy. The model then arises as a weighted geometric average of these two viscosities, namely:

$$\nu_t = C_M(|\overline{S}|)^{\alpha}q^{1-\alpha}\overline{\Delta}^{1+\alpha} \tag{5}$$

where α is a weighting factor in the range 0–1 and C_M a constant. In the computations below, the values $C_M = 0.1$ and $\alpha = 0.5$ have been used. As the SGS energy q is not immediately available, it is estimated by a filtering operation over the test filter $\widehat{\overline{\Delta}}$, equivalent to that adopted for the dynamic model, i.e.

$$q = 0.5\overline{u}_i'\overline{u}_i' \quad \text{with} \quad \overline{u}_i' = \overline{u}_i - \widehat{\overline{u}_i} \tag{6}$$

Because of the manner in which q is determined, the model ensures a monotonic decay of the SGS viscosity as the wall is approached and vanishing eddy-viscosity level in non-turbulent conditions. It shares this property with the dynamic form of the model, but is considerably simpler.

The WALE, proposed by Ducros et al. (1998), is specifically designed to return the correct wall-asymptotic y^{+3}-variation of the SGS viscosity (Hinze, 1975). The model determines the viscosity from

$$\nu_t = C_w\overline{\Delta}^2\frac{\left(\overline{S}_{ij}^d\overline{S}_{ij}^d\right)^{3/2}}{\left(\overline{S}_{ij}\overline{S}_{ij}\right)^{5/2} + \left(\overline{S}_{ij}^d\overline{S}_{ij}^d\right)^{5/4}} \tag{7}$$

where $\overline{S}_{ij}$ is the strain-rate tensor,

$$\overline{S}^d_{ij} = \tfrac{1}{2}\left(\overline{g}^2_{ij} + \overline{g}^2_{ji}\right) - \tfrac{1}{3}\delta_{ij}/\overline{g}^2_{kk} \tag{8}$$

is the traceless symmetric part of the tensor $\overline{g}^2_{ij} = \overline{g}_{ik}\overline{g}_{kj}$, with $\overline{g}_{ij} = \partial\overline{u}_i/\partial x_j$, and $C_w = 0.1$.

3.3. The scale similarity model and the dynamic mixed model

The scale similarity model (SSM) (Bardina et al., 1980) represents the SGS term by the modified Leonard term $L^m_{ij} = \overline{\bar{u}_i\bar{u}_j} - \bar{u}_i\bar{u}_j$. Filtering denoted by the upper bar is, in contrast to the first filter, an explicit operation with filter width equal to the grid spacing. This is implemented in the form of three one-dimensional filters, one in each coordinate direction, with weights 1/8, 6/8, 1/8, as proposed by Zang et al. (1993). This model circumvents the use of a SGS viscosity and thus admits back-scattering. Experience shows, however, that the model is not sufficiently dissipative, so that an additional eddy-viscosity term is needed. The augmented model then arises as (Bardina et al., 1980):

$$\tau^a_{ij} = (L^m)^a_{ij} - 2\nu_t\overline{S}_{ij} \tag{9}$$

Despite the addition of the eddy-viscosity term, backscatter is still effective when the Leonard term dominates. The coefficient determining the magnitude of the eddy viscosity in $\nu_t = C_s\Delta^2|\overline{S}|$ can be calculated by means of the dynamic procedure to finally yield the DMM (Zang et al., 1993). Again, averaging is performed over homogeneous directions, and the total viscosity is constrained to be positive.

4. Near-wall treatment

4.1. Rationale and overview

At high Reynolds numbers, LES cannot resolve the eddies in the semi-viscous near-wall region, unless a very fine mesh is used. Even if such a fine mesh could be accommodated normal to the wall, the reduction in the turbulent scale in all three directions implies the need for similar refinements in the other two directions. This is not tenable on economic grounds and necessitates the adoption of an approximate treatment which bridges the near-wall layer.

Alternative approaches are based on the use of conventional low-*Re* turbulence models or semi-analytical "wall laws". The former approach, realised most conspicuously in Spalart's "detached eddy simulation" strategy (Spalart et al., 1997) interfaces the near-wall RANS and LES regions at a position determined locally by the grid, especially the wall-parallel cell dimensions which may be constrained by wall-remote resolution requirements. Typically, this position is quite close to the wall, often not far above the buffer layer. With a wall function, the wall-parallel spacing is of no consequence, and the use of a blended function, valid over the entire near-wall layer, allows the interface to be placed at any distance normal to the wall by choosing the size of the wall-adjacent grid cell.

In essence, a wall-law approximation is required to return the correct instantaneous wall-shear stress corresponding to the known instantaneous velocity at the wall-nearest computational node. The wall-shear stress is then used as the wall boundary condition in conjunction with the impermeability condition. Usually, the grid point closest to the wall needs to be located in the log-law region, beyond the semi-viscous sublayer. However, more general formulations exist, which do not impose this constraint, as they are constructed based on a composite relation $u^+(y^+)$ applicable across the entire near-wall layer. This is of particular advantage in separated flows in which y^+ varies greatly across the near-wall grid plane, assuming very small values at separation and reattachment points (which also vary in time, of course).

Two different methods have been presented in the literature. Both are based on the assumption that the instantaneous near-wall velocity is in phase with the instantaneous wall shear stress. In Schumann's method (Schumann, 1975), the wall shear stress is taken proportional to the instantaneous near-wall velocity, the proportionality factor being the ratio of the time-averaged values of the two. An evident disadvantage of the method is that it relies on statistical information which needs to be derived from the simulation itself. The other technique is to use a wall law to directly relate the instantaneous velocity at the first grid point in the interior of the flow to the instantaneous shear stress.

In the present study, the latter approach has been adopted. Five different wall laws have been investigated:

- a two-layer log-law (LL2), with the wall-shear velocity used as the velocity scale;
- a three-layer log-law (LL3), similar to LL2 but accounting for the continuous transition between the 'fully-viscous' and 'fully-turbulent' layers;
- a two-layer log-law, with the turbulence energy used as a velocity scale (LLK);
- a 1/7th power-law based formulation blended with a linear near-wall law (WW);
- a formulation combining the Werner–Wengle treatment for forward near-wall flow with a back-flow model with scaling extracted from the reverse-flow region (back-flow, BF).

The following subsections summarise the principal elements of the wall-laws.

4.2. Log-law-based approximations

The simplest formulation (LL2) is based on the assumption that the near-wall layer consists (in an instantaneous sense) of a fully viscous sublayer and a fully turbulent superlayer with the interface defined by $y^+ \leqslant 11$. Thus,

$$u_1^+ = \begin{cases} y_1^+ & \text{if } y_1^+ \leqslant 11 \\ \kappa^{-1}\ln(Ey_1^+) & \text{if } y_1^+ > 11 \end{cases} \tag{10}$$

with $\kappa = 0.42$ the von Karman constant, $E = 9.8$, $u_1^+ = u_1/u_\tau$, $u_\tau = \sqrt{\tau_w/\rho}$ and $y_1^+ = y_1 u_\tau/\nu$. Here, u_1 is the resolved velocity tangential to the wall at the wall-nearest point, and y_1 the distance of this point from the wall. To be of use as a boundary condition in a simulation, relation (10) is assumed to hold in an instantaneous sense, so that the instantaneous shear stress can be deduced from y_1 and u_1.

The profile given by (10) exhibits a kink at $y_1^+ = 11$, which is unrealistic. To account for the smooth transition between the linear and the logarithmic region in the buffer layer, observed in experiments and DNS, a logarithmic fit can be used in the buffer layer, resulting in the following three-layer (LL3) law (Breuer and Rodi, 1996):

$$u_1^+ = \begin{cases} y_1^+ & \text{if } y_1^+ \leqslant 5 \\ A\ln(y_1^+) + B & \text{if } 5 < y_1^+ \leqslant 30 \\ \kappa^{-1}\ln(Ey_1^+) & \text{if } y_1^+ > 30 \end{cases} \tag{11}$$

with $A = (\kappa^{-1}\ln(30E) - 5)/\ln(6)$ and $B = 5 - A\ln(5)$.

In the above log-laws, the velocity scale in y^+ is formed with the wall-shear stress. This form therefore establishes a rigid linkage between the near-wall velocity and the wall-shear stress and gives a seriously erroneous wall shear stress if the near-wall flow departs significantly (in a Reynolds-averaged sense) from the state of turbulence-energy equilibrium. In RANS computations, the validity of the log-law has been extended considerably by using the turbulence energy, rather than the shear velocity, to scale y. This substitution is based on the equivalence $u_\tau^2 = C_\mu^{0.5} k$ which is strictly valid only in the presence of turbulence-energy equilibrium (Launder and Spalding, 1974). This concept has been applied to LES (Murakami et al., 1993; e.g.) with $k = k_1$ being the resolved turbulence energy at the wall-nearest node. For this approach (LLK), the universal wall distance thus arises as:

$$y_1^+ = yC_\mu^{1/4}k_1^{1/2}/\nu \tag{12}$$

with $C_\mu = 0.09$ and

$$k = 0.5\langle(\overline{u_i} - \langle\overline{u_i}\rangle)(\overline{u_i} - \langle\overline{u_i}\rangle)\rangle = 0.5(\langle\overline{u_i u_i}\rangle - \langle\overline{u_i}\rangle\langle\overline{u_i}\rangle) \tag{13}$$

where $\overline{u_i}$ is the instantaneous velocity while $\langle\cdot\rangle$ indicates an averaging operator in time and in any homogeneous direction present. Otherwise, the wall law is identical to that given by Eq. (10).

A disadvantage of approximation (12) is that it requires the resolved near-wall turbulence energy, which is, however, part of the solution. In practice, this energy is determined from 'on-the-run' time-averaging as the simulation progresses. This average stabilizes fairly quickly, well before the collection of statistical data commences by ensemble-averaging. Hence, the penalty in terms of computing resource is minimal.

Any of the above forms may be implemented, computationally, in two ways. The simpler (default) route is to determine the wall-shear stress upon a direct substitution of the resolved wall-parallel velocity at the wall-nearest node into the assumed near-wall profile. The other route is based on the notion, consistent with the finite-volume method, that the resolved velocity at the wall-nearest node is the average value over the associated cell. Hence, the assumed near-wall profile is integrated in wall normal direction from which then a relationship is obtained between the *cell-averaged* and the wall-shear velocities. The wall-shear stress then follows from a substitution of the resolved near-wall velocity into this integral relationship. Both approaches can be defended, although the latter can be argued to be inconsistent with the order of the (linear) approximations used to determine the numerical fluxes on the finite-volume faces. For a linear velocity profile (i.e. when the near-wall cell is wholly within the viscous sublayer), both implementations give identical wall-shear-stress values. However, significant differences can arise when the cell extends into the buffer and turbulent layer where the velocity profile is highly non-linear. This sensitivity will be illustrated below through simulations undertaken with the two-layer wall-law used in its default, 'point-wise' form (LL2) and in its cell-integrated form (LL2-i).

4.3. The Werner–Wengle wall law

The log-law, if used exclusively with the shear velocity, is trancendental and requires an iterative inversion for the wall shear stress. On the other hand, the alternative of using k in y^+ renders the wall-law quasi-explicit, but requires the evaluation of the resolved turbulence energy. Both forms are computationally cumbersome. A simpler two-layers approximation, proposed by Werner and Wengle (1991), is based on the assumption of a 1/7th power-law outside the viscous sublayer, interfaced with the linear profile in the viscous sublayer (WW):

$$u_1^+ = \begin{cases} y_1^+ & \text{if } y_1^+ \leqslant 11.8 \\ 8.3(y^+)^{1/7} & \text{if } y_1^+ > 11.8 \end{cases} \tag{14}$$

Werner and Wengle (1991) propose the use of the integrated form of the above profile over the near-wall cell—a default implementation denoted by WW and explained in the previous section by reference to LL2-i. While this option has been adopted in most simulations to follow, one simulation, denoted by WW-p, has been performed in which the wall-shear stress was obtained directly from Eq. (14), i.e. through a point-wise substitution. The comparison between the simulations using WW and WW-p thus complements the analogous comparison between the simulations performed with LL2-i and LL2.

4.4. The backflow wall law

With all wall functions discussed so far, no particular assumption on the direction of the flow is implied. Thus, the tangential velocity vector is computed, yielding the corresponding shear stress, which is then decomposed into grid-oriented components. Hence, these laws also work, numerically, for reverse flow. However, physically, the wall-scaling applied to simple boundary-layer flows is not valid within the near-wall, reverse-flow layer of a recirculation bubble.

The analysis of separating, recirculating flow (Simpson, 1983; Devenport and Sutton, 1991) suggests that the characteristic scales for velocity and length within the recirculation region are, respectively, the maximum average backflow U_N and and the distance of this maximum y_N from the wall. The characteristic Reynolds number is then $Re^* = y_N U_N/\nu$. The values U_N, y_N, and hence Re^*, can be determined locally for each grid point on the wall by a search in wall-normal direction.

In Mathey et al. (2002), the relation

$$U^* = C_\kappa(y^* - \log(y^*) - 1) \tag{15}$$

has been proposed, where $U^* = (U + U_N)/U_\tau$ and $y^* = y/y_N$, with U denoting the near-wall average tangential velocity. Comparisons with simulation data, similar to those in Fig. 9, have shown that the value $C_\kappa = 1/\kappa$ ($\kappa = 0.41$) gives a good representation of the data. This equation turned out to be computationally ill-conditioned, however, and hence impractical for use as a boundary condition in the simulations. As a stable alternative, the following direct relationship between Re^* and $c_f^* = 2\tau_w/\rho U_N^2$ has thus been devised (Mathey et al., 2002):

$$Re^* = \begin{cases} C_\kappa\sqrt{2/c_f^*}\left(\mathrm{e}^{\kappa\sqrt{2/c_f^*}} - 1\right); & Re^* > Re_c^* \\ 2.41\left(2/c_f^*\right)^{1.087}; & Re^* < Re_c^* \end{cases} \tag{16}$$

The value $Re_c^* = 75.1$ for the intersection has been chosen so as to yield an overall continuous function. The low-Re^* part is the empirical formula of Le et al. (1997) which is close to the laminar relation. This is used when the grid is sufficiently fine to resolve the viscous sublayer. In regions of forward flow, the Werner–Wengle model is applied. The blending between both is quite natural and accomplished by just switching from one to the other relation for the wall-shear stress. The distinction between forward and backward flow is made according to the direction of the flow at the wall-adjacent grid node, the main flow in the channel serving as a reference. The above implementation is denoted by BF in results to follow.

5. Numerical framework

5.1. The STREAMLES code

STREAMLES is one of two entirely independent codes used to generate the results reported in the present study. The code, developed by Lardat and Leschziner (1998), applies to incompressible flow and uses a non-orthogonal finite-volume procedure with collocated, cell-centred storage of all flow properties and cartesian velocity components. The numerical scheme is based on a fractional-step method, with the time derivative being discretised by a second-order backward approximation. The convection and diffusion terms, approximated by centred schemes of second-order accuracy, are advanced in time using the Adams-Bashfort method. The pressure is obtained as a solution of the pressure-Poisson problem by means of a partial-diagonalisation technique (Schumann and Sweet, 1988) and a V-cycle multigrid algorithm operating in conjunction with a successive line over-relaxation scheme. Updates of the intermediate cell-centred and contravariant cell-face velocities are then effected via two different, respective representations of the discrete pressure gradient in a manner akin to that proposed by Rhie and Chow (1983). STREAMLES is fully parallelized and has been run on up to 256 Cray T3E processor partitions at efficiencies of the order of 90%. Parallel-performance aspects of the code, relating to several computer architectures, are discussed in Temmerman et al. (2000).

5.2. The LESOCC code

Large eddy simulation on curvilinear coordinates (LESOCC) is a general, multi-block, finite-volume scheme developed by Breuer and Rodi (1994, 1996); Mathey et al. (1999) and Mellen et al. (2000) for the solution of the incompressible-flow equations. Its basic cell and storage arrangements are very similar to those of STREAMLES, as is the centred, second-order spatial discretisation of the convective and viscous fluxes. In contrast, however, time advancement is effected by an explicit, low-storage Runge–Kutta method. Conservation of mass is achieved by the SIMPLE algorithm, with the pressure-correction equation being solved by the SIP

procedure of Stone (1968). The momentum-interpolation method of Rhie and Chow (1983) is employed to prevent pressure–velocity decoupling and associated oscillations.

6. Plane channel flow simulations

As a precurser to the study of separated periodic hill flow, simulations for fully-developed channel flow were undertaken for two reasons: first, to investigate the performance of alternative subgrid-scale models, thus allowing the selection of one principal model for use in the separated hill flow; second, to examine the ability of alternative wall laws to return the log-law behaviour with coarse near-wall grids for a Reynolds number that is comparable to that of the hill flow.

Simulations were performed for friction Reynolds numbers in the range $180 \leqslant Re_\tau \leqslant 1050$, the upper limit corresponding to a mean-flow Reynolds number of 21000. Attention focuses here on the case $Re_\tau = 590$ for which DNS solutions by Moser et al. (1999) are available for comparison. Most wall-resolving simulations were done on a grid containing $96 \times 64 \times 64$ nodes, covering a box of $2\pi h \times 2h \times \pi$ h and giving cell sizes in wall units of ($\Delta x^+ = 38$, $\Delta y^+ = 2 - 42$, $\Delta z^+ = 29$), the lower limit $\Delta y^+ = 2$ being that at the wall. With this cell size, the first grid point is at $y_1^+ = 1$ from the wall. Statistical properties were assembled over a period of 12 flow-through times, sufficient to ensure fully converged levels.

Excluding wall-function simulations, which will be considered later, a total of six modelling practices were adopted, SM, SM-WD, DSM, LDSM, MSM, and WALE, as discussed earlier (see also Table 1). Performance was judged by reference to mean velocity, shear Reynolds number and Reynolds-stress components, all relative to the DNS solution. These comparisons, not included here, suggested that the SGS viscosity returned in the buffer region was especially influential, consistent with the fact that the SGS viscosity was of the same order as the molecular viscosity. Fig. 3 demonstrates that different models return materially different SGS viscosity distributions. The logarithmic scale, adopted to enhance the near-wall variations, somewhat obscures the fact that the maximum viscosity values, occuring in the log-law layer, vary within a range of about one order of magnitude, between 0.1 and 1 times the fluid viscosity, with the WALE model returning the lowest value and the LDSM the highest. However, this difference is not in itself influential because the SGS transport is a small proportion of the resolved transport in the log-law region. Of greater importance is the viscosity level in the upper portion of the buffer layer and the rate of change in the SGS viscosity within the buffer layer as a whole. It has been observed that high SGS viscosity in the region $10 < y^+ < 20$ tends to depress the velocity in the buffer and log regions below the DNS variation, while the reverse occurs when the viscosity in this region is low.

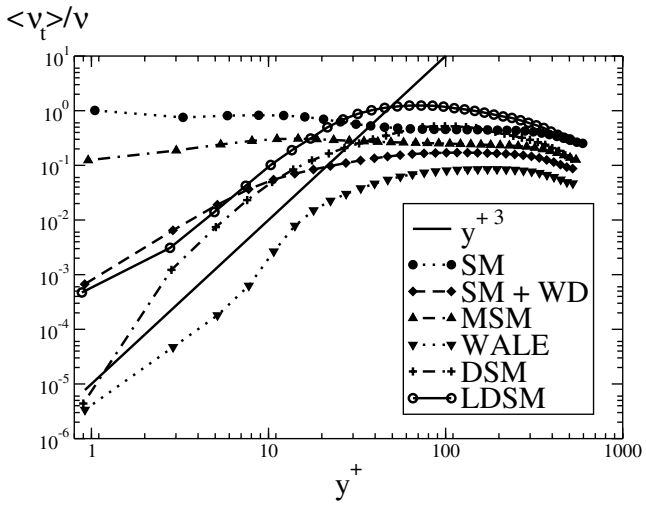

Fig. 3. Subgrid-scale viscosity in channel flow, $Re_\tau = 590$; sensitivity to SGS modelling.

The theoretical wall-asymptotic behaviour is cubic in y^+, represented by the straight line in Fig. 3. The only two models of those employed that return this variation reasonably well are the WALE model and the Dynamic variants, although the magnitudes of SGS viscosity these models give away from the wall differ substantially. While the precise rate of decay in the viscous sublayer is not of major importance, in view of the very low levels of the viscosity, it is important that the decay is reproduced broadly correctly in order to ensure that the SGS viscosity becomes, as it should be, an insignificant proportion of the fluid viscosity. Overall, the WALE model was found to return the best velocity distribution, although the representation of the buffer region is not entirely satisfactory.

The performance of the wall laws described in Section 4 is examined here for the same channel flow as above, but with a deliberately coarsened grid containing $64 \times 32 \times 32$ cells. The cell dimensions in wall units are (Δx^+, Δy^+, Δz^+) = (58, 37, 58). All wall formulations were used in combination with the WALE SGS model. Table 2 gives errors in wall-shear Reynolds number and centreline velocity relative to the DNS. Velocity and turbulence-intensity profiles are given in Figs. 4 and 5.

Table 2
Wall shear stress and centreline velocity for channel flow; wall-function simulations

SGS and wall model	Re_τ	Error to DNS (%)	u_c/U_b	Error to DNS (%)
DNS	584	–	1.1418	–
WALE + LL2	558.5	−4.4	1.12	−1.91
WALE + LL3	557.8	−4.5	1.118	−2.08
WALE + LLK	537.6	−7.9	1.13	−1.03
WALE + WW	598.4	2.5	1.133	−0.08

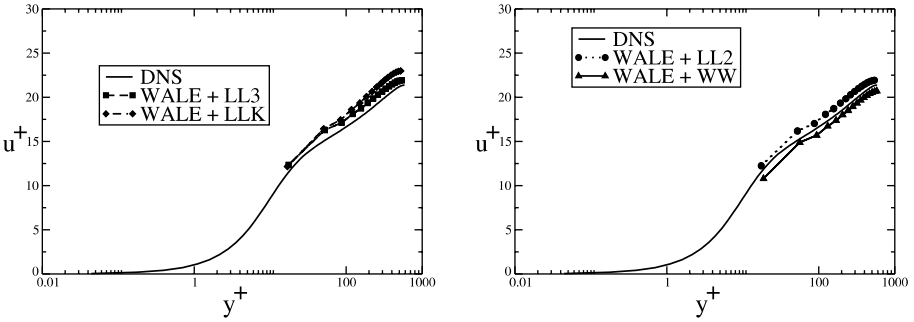

Fig. 4. Streamwise velocity in channel flow; sensitivity to near-wall treatment.

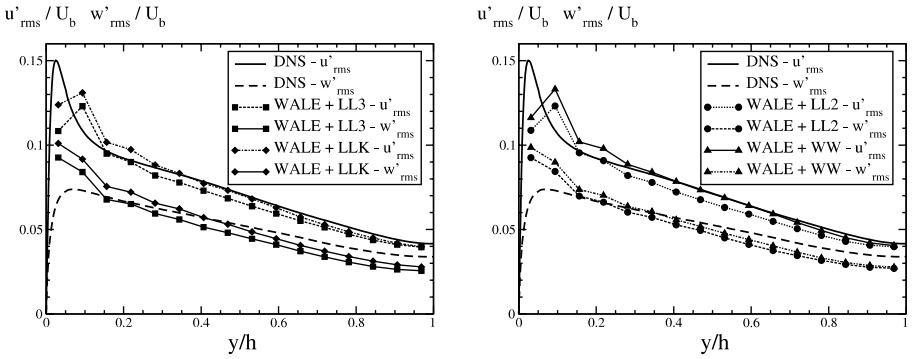

Fig. 5. Turbulence intensities in channel flow; sensitivity to near-wall treatment.

Considering the coarseness of the grid used, the results are certainly not disappointing, especially in terms of the resolution of the velocity and turbulence intensities away from the wall, over 80% of the channel width. Table 2 shows that the three log-law formulations slightly underpredict the wall-shear velocity, leading to the log-law profile (see Fig. 4) lying slightly above the DNS solution, while the Werner–Wengle formulation returns the opposite behaviour, but gives results quite close to the DNS solution. A degree of uncertainty arises here from the fact that the log-laws were implemented so as to yield the wall-shear stress using, directly, the velocity u_1 at the wall-nearest node y_1, while the WW model involved the cell integration described in Section 4.3; both are the default implementations. This may be the reason for the offset in the wall-nearest velocity seen in Fig. 4.

The turbulence intensities (Fig. 5) are reasonably well predicted. Based on the results presented and additional observations not discussed herein, the Werner–Wengle formulation was judged to give, overall, the best performance, and this led to its preferential adoption for most of the hill-flow calculations considered below.

7. Highly-resolved simulations

The absence of experimental data for the periodic-hill flow necessitated the generation of a reference database extracted from reliable simulations for that flow. Two such simulations were performed, independently, using the two independent codes described in Section 5. The same mesh of close to 4.6×10^6 ($N_x \times N_y \times N_z = 196 \times 128 \times 186$) interior cells was employed in both cases. This high-quality mesh—designated "Grid 3" in the discussion to follow—is close to orthogonal and of low aspect ratio over most of the domain. The mesh-expansion ratio does not exceed 1.05, and the wall-nearest computational point is located, in terms of wall units, at a value of about 0.5 over most of the lower wall. At the upper wall, a wall-function approach was adopted for cost reasons. This is of little consequence to accuracy, however, as the detailed viscous features of the flow near the upper wall are neither of interest here nor of any importance to the lower portion. Subgrid-scale effects were represented by the WALE model in STREAMLES and the DSM in LESOCC. Despite the high resolution, especially in the separated lower part of the flow, this difference is not entirely unimportant, because the intense turbulence activity in the separation zone tends to give rise to a moderate level of SGS viscosity, especially when the DSM model is used. Statistics were assembled for a period of 55 flow-through times. These simulations and their analysis, including considerations on stress budgets, realisability maps and spectra, are the subject of the companion paper (Mellen et al., 2002b). Here, only some key facts are reported to provide a sufficient

background for the coarse-grid study presented in the next section.

A general view of the flow is conveyed in Fig. 1. The plot shows a highly unsteady shear layer downstream of the crest of the hill and the vortical motion which is generated by the Kelvin–Helmholtz instability. Animations of the flow show the vortices to break up and to undergo helical pairing. The mean streamlines in Fig. 1 demonstrate that reattachment occurs, as intended when defining the geometry, on the lower plane channel wall, well upstream of the next hill (see Table 3 for the exact locations and note also the referencing system). As observed in Section 2, this feature results in an especially sensitive response of the recirculation zone to the resolution of processes around the separation point and in the separated shear layer, thus making this flow a searching test case for the adequacy of coarse-grid LES and the attendant approximations.

The level of agreement between the two highly-resolved solutions is exemplified by Fig. 6 showing profiles of the mean streamwise velocity and the corresponding shear and normal stress (note that symbols are used here and in following figures to distinguish lines and do not indicate mesh nodes). The position has been selected so as to show the point of maximum difference. At other locations, such as $x/h = 6.0$, the agreement is substantially better (Mellen et al., 2002b). The velocity profiles are clearly very close, while differences in the normal-stress profiles are somewhat larger. In part, this is due to differences in the level of the respective subgrid-scale viscosity shown in Fig. 7. As observed in other simulations of plane channel flow, the WALE model tends to give considerably lower viscosity values than the DSM, and this is also the case for the hill flow. While both models return fairly low SGS viscosity levels, the maximum viscosity ratio of order 2 predicted by the DSM reflects the intense turbulence activity in the separation and post-reattachment zones close to the wall, and this has a non-negligible effect on the simulated quantities. The present simulations nevertheless provide a sufficiently accurate foundation for assessing approximate near-wall treatments in coarser-grid LES. As will be seen in the next section, the differences arising from different near-wall treatments are substantially larger than those between the two highly-resolved simulations.

Of particular interest in the context of the study of near-wall approximations are the wall-parallel velocity profiles expressed in terms of wall coordinates. Five such profiles, extracted from the simulation at different streamwise locations at the lower wall, are shown in Fig. 8 in comparison with the standard log-law. Obviously, the profiles are remote from the log-law, and this is already indicative of the anticipated difficulties in using related wall-functions in the coarse-grid simulations to be considered in the next section. While the absence of a log-law in the separated region is not surprising, Fig. 8 demonstrates that no part of the reattached-flow profile at $x/h = 6$ conforms to the log-law either. Further downstream, there is a trend towards a re-establishment of the log-law, but this ceases when the flow accelerates strongly on the wind-ward slope of the next hill. This is,

Table 3
Overview of computations discussed in the present paper

Case	Grid	SGS	Wall	Code	$(x/h)_{sep}$	$(x/h)_{reat}$
1	1	WALE	NS	STREAMLES	1.12	2.17
2	1	WALE	WW	STREAMLES	0.46	4.00
3	1	WALE	WW-p	STREAMLES	0.52	3.059
4	1	WALE	LL2	STREAMLES	0.54	2.95
5	1	WALE	LL2-i	STREAMLES	0.41	3.95
6	1	WALE	LL3	STREAMLES	0.53	2.98
7	1	WALE	LLK	STREAMLES	0.49	3.38
8	1	SM + WD	WW	STREAMLES	0.50	3.59
9	1	MSM	WW	STREAMLES	0.45	4.18
10	1	LDSM	WW	STREAMLES	0.47	3.56
11	1	SM + WD	WW	LESOCC	0.45	3.60
12	1	DSM	WW	LESOCC	0.50	3.20
13	1*	DSM	WW	LESOCC	0.45	3.25
21	2	WALE	NS	STREAMLES	0.38	3.45
22	2	WALE	LL3	STREAMLES	0.34	4.32
23	2	DSM	BF	LESOCC	0.37	4.14
24	2	WALE	WW	STREAMLES	0.32	4.56
25	2	SM + WD	WW	LESOCC	0.32	4.70
26	2	DSM	WW	LESOCC	0.30	4.23
27	2	DMM	WW	LESOCC	0.30	3.85
31	3	WALE	NS	STREAMLES	0.22	4.72
32	3	DSM	NS	LESOCC	0.20	4.56

The abbreviations for subgrid-scale and wall models are defined in Table 1. Case 13 is identical to Case 12 but, with twice the distance and grid planes in the spanwise direction.

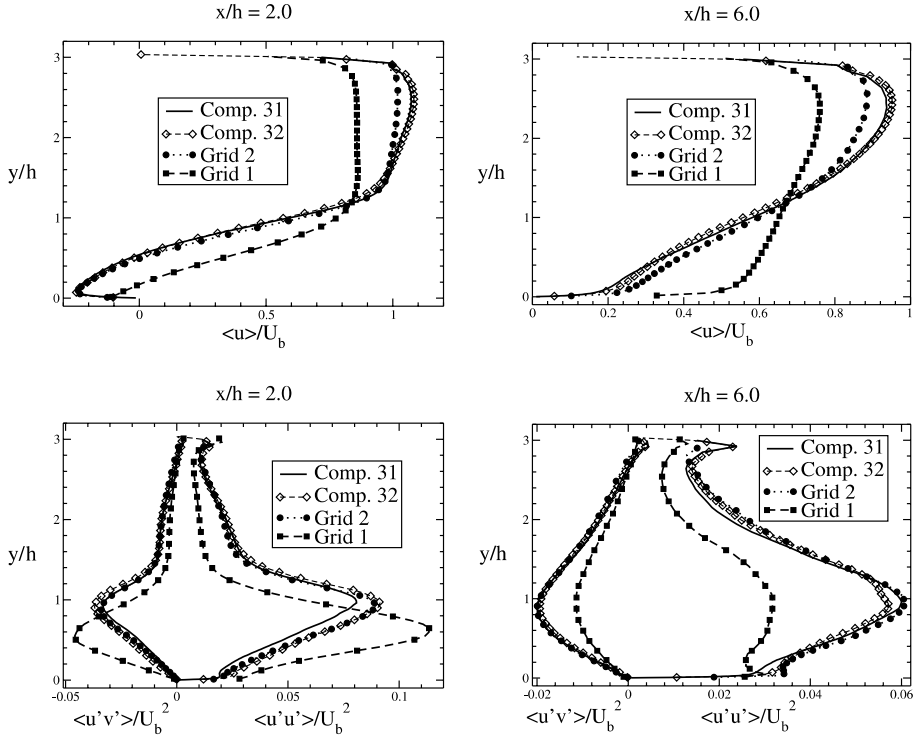

Fig. 6. Streamwise velocity, resolved streamwise stress and resolved shear stress at $x/h = 2$ and 6 for Grids 1, 2 and 3, the WALE model and the NS wall condition have been used in all cases except for simulation 32 which used the DSM model.

thus, clearly a highly disturbed flow in which the near-wall layer is not given an opportunity to recover to a near-universal state—a condition aggravated by the relatively low Reynolds number for which the semi-viscous sublayer is relatively thick.

The fully-resolved simulations also allow an a priori examination of the validity of the scaling underlying the backflow wall function described in Section 4.4. Fig. 9 compares the profile provided by Eq. (15) against corresponding profiles extracted from the simulation at five locations within the recirculation zone. As seen, the backflow scaling is appropriate over most of the recirculation zone. Close to the separation and reattachment points, the recirculation bubble becomes small and effectively collapses into the wall-adjacent cell, so that the determination of the reference quantities and hence matching become difficult. This issue is further discussed below.

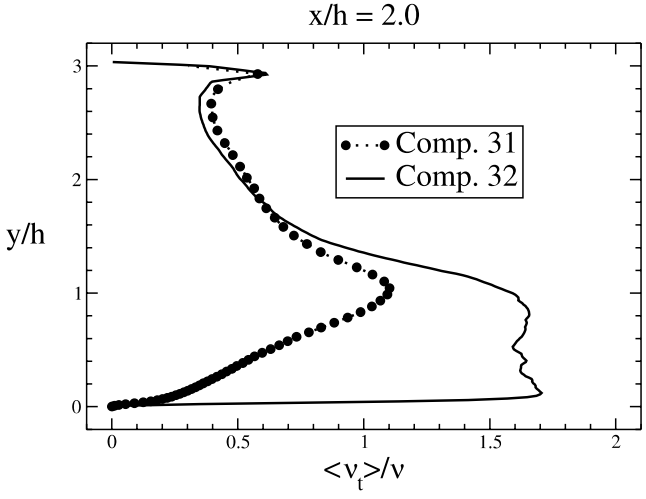

Fig. 7. SGS viscosity at $x/h = 2$ for highly-resolved simulations 31 and 32.

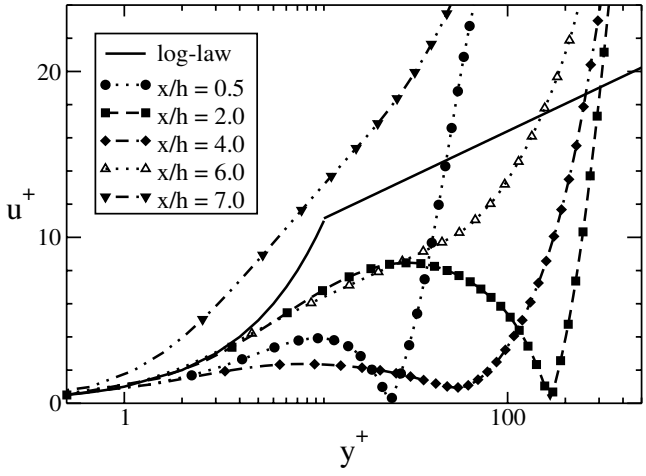

Fig. 8. Near-wall velocity profiles at five streamwise locations derived from the highly-resolved simulation 31.

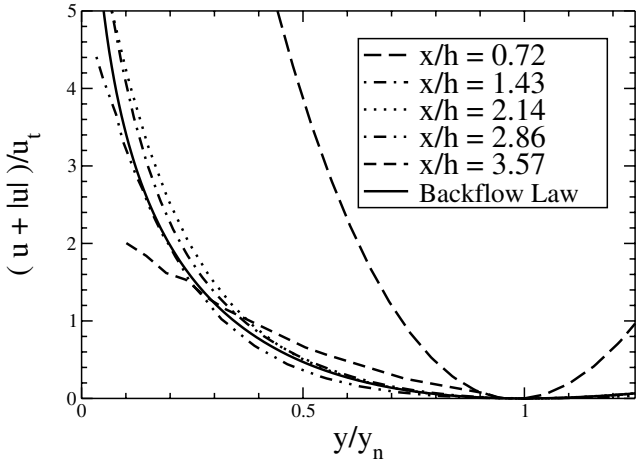

Fig. 9. Near-wall backflow-scaled velocity profiles at five locations within the recirculation zone, derived from the highly-resolved simulation 32. The velocity scaling according to Eq. (15) is applied to the simulation data while the continuous line represents Eq. (15) itself.

8. Coarse-grid LES with near-wall approximations

8.1. Overview

The principal purpose of this study is to convey insight into the predictive accuracy that can be achieved by simulations of flow separating from curved surfaces with grids deemed 'economically tenable' in a practical environment. Although the separated flow under consideration is challenging, it must be born in mind that its Reynolds number is still relatively low, and hence the conditions simulated are fairly 'benign'—say, in comparison to a separated wing flow at a typical Reynolds number of 10^7. Real engineering flows are much more demanding, and the sensitivity levels reported below are likely to be considerably more severe in practice.

The range of simulations undertaken is summarised in Table 3 (for abbreviations see Table 1). These simulations were conducted along three parametric 'axes' intended to allow the contribution of resolution, SGS modelling and near-wall approximation to be separated, at least qualitatively. Simulations 1–13 have been performed on Grid 1, shown in Fig. 2 ($112 \times 64 \times 92 = 0.66 \times 10^6$ interior cells). Of these, simulations 1–7, all done with the WALE SGS model, are designed to convey the sensitivity of the solution to the near-wall treatment—including the two implementation options explained in Sections 4.2 and 4.3, while simulations 8–12, all undertaken with the Werner–Wengle wall function (WW), are intended to bring out the dependence of the solution on subgrid-scale modelling for that grid. Simulation 13 is identical to 12, except for the spanwise extent and the number of spanwise grid planes, both of which have been doubled in the former case to examine spanwise decorrelation. Simulations 21–27 form a selection from set 1–10 for the finer Grid 2, shown in Fig. 2 ($176 \times 64 \times 92 = 1.04 \times 10^6$ interior cells). Computation 23 was specifically designed to examine the advantages gained from using the backflow wall function in the recirculation zone. Finally, cases 31 and 32 identify the highly-resolved simulations which are the subject of Section 7. All three grids employed in the current study have been produced with an in-house grid-generation programme based on the solution of an elliptic equation with forcing terms adjusted so as to steer the positioning of nodes. This yields smooth and almost orthogonal grids, which is particularly beneficial in the context of LES.

In Table 3, the two right-most columns give the predicted time-mean separation and reattachment locations, obtained upon integration over at least 50 flow-through times. These allow a number of interesting points to be highlighted, ahead of the detailed discussion of field data. First, it is observed that the recirculation length varies greatly with mesh, wall-treatment and SGS model: the shortest recirculation length is about 2 hill heights, in comparison to 4.5–4.7 returned by the highly-resolved simulations. Second, attention is drawn to the correspondence between simulations 8 and 11, both performed with the Smagorinsky model and the Werner–Wengle wall function, but with different codes. Third, it is noted that doubling the spanwise extent (case 13 relative to 12) only results in a very minor change in the predicted separation and reattachment points. This reflects the fact, already noted in Section 2, that spanwise correlation decays to insignificant levels, over most of the flow, within a spanwise distance of 2 hill-heights. Forth, the flow is evidently fairly sensitive to the implementation details of any one of the wall-laws. Thus, the simulation pairs $(2,3)$ = (WW,WW-p) and $(4,5)$ = (LL2,LL2-i) demonstrate a consistent difference between the integrated and point-wise implementations, with the former practice yielding a significantly longer recirulation zone, in better accord with the highly-resolved solution. Finally, as shown in Fig. 10, there is a fairly strong correlation between the separation and reattachment locations: typically, a forward shift of the separation point by 0.15 hill heights results in a shortening of the recirculation zone by 1 hill height—a causal relationship which will be revisited below. This brings out an important difference between simulating a flow in which separation is fixed by edges, relative to one in which separation occurs from a continuous surface, especially when reattachment is not enforced by a geometric feature or blockage causing early reacceleration.

8.2. Effects of resolution

Compared to the dense Grid 3, used for the highly resolved simulations 31 and 32 in Table 3, two substantially coarser grids have been used to investigate

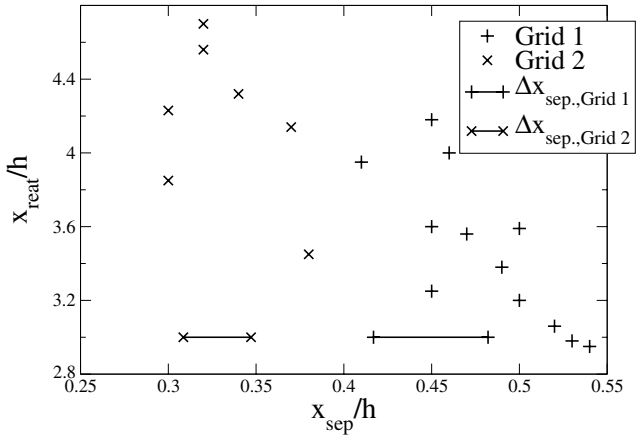

Fig. 10. Correlation between separation and reattachment locations, + identifies data obtained with Grid 1, × identifies data obtained with Grid 2. The lines indicate the streamwise internodal distance (normalised by h) in the separation region.

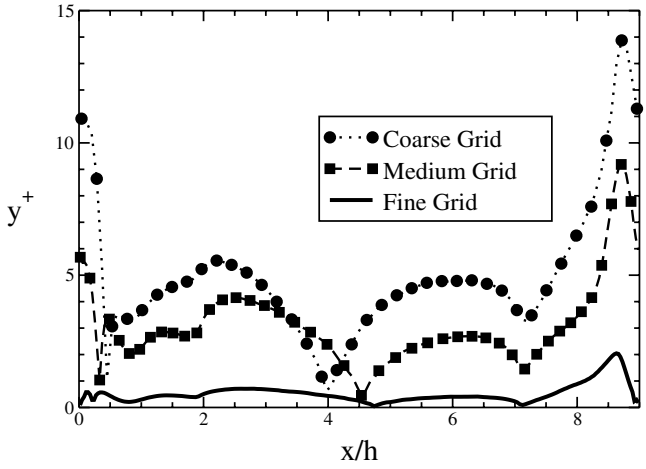

Fig. 11. Universal wall-distance along the line passing through the centre of the wall-adjacent cells close to the lower walls; from simulations 1 and 21 using the WALE SGS model and the WW wall function.

issues of resolution and modelling. The coarsest 'Grid 1' (0.66×10^6 cells) has a fairly uniform density over the domain. The medium 'Grid 2' is moderately finer (1.04×10^6 cells), but the refinement was introduced preferentially around the hill crest, and the nodes were redistributed in the y-direction so as to achieve a better resolution at the lower wall.

An impression of the difficulties that are posed by using 'coarse' grids for separated flow is conveyed by Table 4, Figs. 6 and 10. Fig. 6 shows profiles of velocity, (resolved) streamwise normal stress and shear stress at two locations, $x/h = 2$ and 6, i.e. within the separation bubble and after reattachment. Results are compared for the three grids employed using the same SGS model (WALE) and the same NS wall condition. This boundary condition might appear inappropriate for the coarsest grid—although it has been used with considerably coarser meshes in wavy-wall simulations (e.g. Salvetti et al., 2001). However, as is evident from Fig. 11, the time-averaged y^+-values corresponding to the distance between the lower wall and the first grid plane are mostly below 8; the peak value of 14 arises at the crest of the hill, following the strong acceleration on the windward side. Thus, while a NS condition is undoubtedly a poor approximation, it might not be expected to be disastrously bad. However, when this condition is used in combination with poor resolution around the separation point, it leads to a serious misrepresentation of the entire flow, principally because of the substantial downstream shift in the separation point. As the wall shear strain is evaluated, in this case, using a linear approximation to the near-wall velocity, the resulting shear stress is underestimated relative to both the real value and that arising from a log-law-based wall function. Hence, following acceleration, flow-retardation by wall shear is inhibited, and separation is thus delayed. Since the separation bubble is much shorter the $\langle u \rangle$-profile at $x/h = 6$ is much fuller, the substantially lower shear strain at that location being compatible with a much lower level of turbulence intensity and shear stress. Upstream of reattachment, at $x/h = 2$, the separated shear layer returned by the coarsest grid is significantly lower and more turbulent than the highly-resolved layer, as is reflected by the higher fluctuation intensity and shear stress. This higher level of turbulence intensity is consistent with the smaller distance between the separation point and the profile location in question ($x/h = 2$), together with the fact that the turbulence intensity reaches a maximum a short distance downstream of the separation location. Hence, it seems clear that the realism of the solution in the vicinity of the separation location is crucially important. An inappropriate downstream shift gives the wrong (mean) separation height and angle, and this, coupled with strong mixing immediately following separation, encourages rapid reattachment.

Table 4
Sensitivity of separation and reattachment locations to grid parameters at the hill crest

Case	$(x/h)_{sep}$	$(x/h)_{reat}$	Grid size ($N_X \times N_Y \times N_Z$)	$(\Delta x/h)_{sep}$	$\Delta x_{crest}/h$	$\Delta y_{crest}/h$	$\Delta z_{crest}/h$
1	1.12	2.17	$112 \times 64 \times 92$	0.065	0.08	0.032	0.049
21	0.38	3.45	$176 \times 64 \times 92$	0.039	0.04	0.02	0.049
31	0.22	4.72	$196 \times 128 \times 186$	0.032	0.032	0.0033	0.024

Evidently, the grid resolution around the hill crest, where separation occurs, is highly influential. Table 4 gives, for the 3 grids employed, the value of the streamwise cell length, Δx around the time-mean separation point and the cell dimensions (in wall units) just above the hill-crest (see also the horizontal line segments in Fig. 10). Although the position of the separation line varies in time within the wide range of $-0.05h$ and $0.7h$, the expectation must be that the separation point cannot be determined to a precision substantially better than the cell length, $0.08h$ in the case of Grid 1. The associated margin in the reattachment location, implied by Fig. 10, is of order $0.5h$, and such a shift results in a substantial change to the entire flow. Thus, subject to uncertainties arising from the crude NS condition used here, it may be stated that grid resolution around the separation location is especially important and, potentially, of major consequence to the predicted gross flow features. As the instantaneous position of separation shifts across a significant portion of the hill surface, adequate grid density must be provided over the entire region in which separation is expected to occur.

8.3. Sensitivity to near-wall modelling on the coarsest grid

Although the streamwise resolution around the separation point is evidently a key factor, the near-wall treatment can also be expected to be a major contributor to predictive accuracy, if only because the near-wall y^+-value in the hill-crest region is high and the separation point is clearly sensitive to the details of the flow conditions in this region.

An overall view of the dependence of the flow on the near-wall approximation, on the coarsest grid, is given in Table 3, cases 1–7. All simulations were performed with the WALE model. Clearly, the separation characteristics are highly sensitive to the near-wall approximation, and this is brought out especially well relative to the NS implementation. In all cases, separation is delayed and reattachment is early. While the latter is linked to the former (see Fig. 10), as discussed in the previous subsection, it is evident that the near-wall approximation also has a direct influence on the reattachment location. This fact is implied, albeit qualitatively, by the scatter in Fig. 10.

Profiles of velocity, streamwise normal stress and shear stress, obtained with the various near-wall approximations, are shown in Fig. 12. All three log-law-based approximations, when implemented in their standard (point-wise) form, return solutions which are better than that obtained with the NS condition, but which are nevertheless far from the highly-resolved simulation, especially in the post-reattachment region. In contrast, the default (cell-integrated) Werner–Wengle approximation (WW) returns a much better solution, which is remarkably close to the highly-resolved simulation. As will be demonstrated below, this is mainly the consequence of the cell-integrated implementation. Of

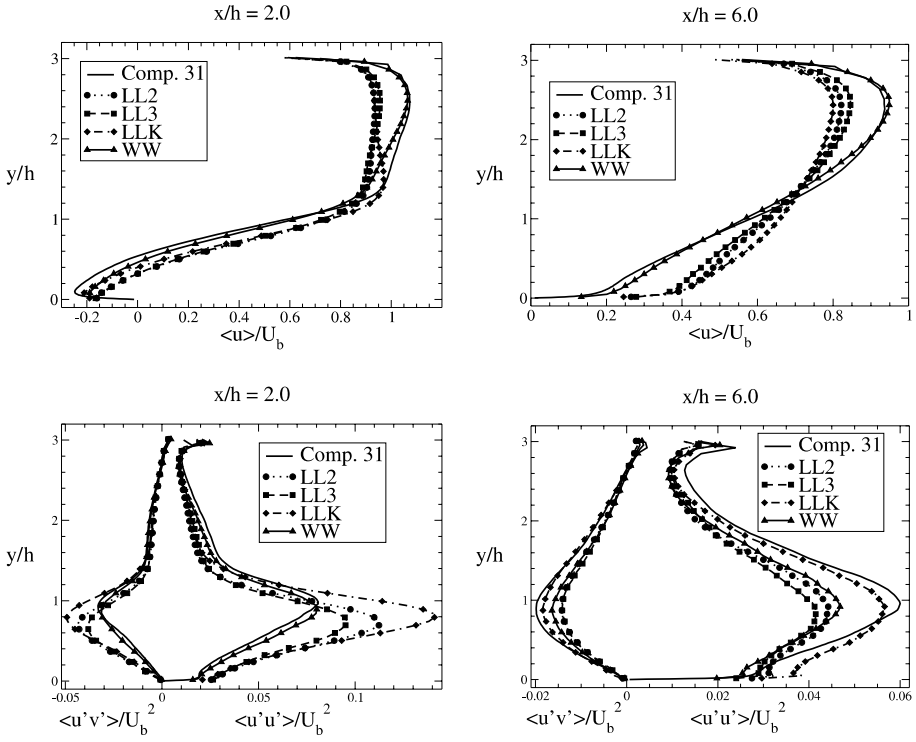

Fig. 12. Streamwise velocity, resolved streamwise stress and resolved shear stress at $x/h = 2$ and 6 using four wall-treatments and the WALE model on the coarsest grid.

the three log-law approximations, that using $\langle k \rangle$ as the velocity scale in the log-law (LLK) offers a modest advantage in terms of the separation and reattachment locations, but not in respect of other quantities. It should be noted that this variant differs fundamentally from the other two in its use of a time-averaged rather than instantaneous velocity scale in the log-law. This effectively established, for any one near-wall cell, a linear relationship between the near-wall velocity and the shear velocity, in the same sense as that established by Schumann's wall law (Schumann, 1975). Moreover, a significant uncertainty with this variant arises from the inaccuracy in determining the near-wall turbulence energy on the coarsest grid use. This is especially problematic in the vicinity of the separation point.

As is the case with the NS implementation, late separation is accompanied by higher turbulence activity in the separated shear layer (at a given x/h location), early reattachment and lower post-reattachment turbulence activity. Although, as argued earlier, a forward shift in the separation location is associated with an increase in turbulence levels at given streamwise x/h positions, this causal relationship is not firm, for some simulations show significant differences in maximum turbulence levels in the shear layer together with quite similar separation locations. This suggests that, at least with the coarse grid used here, separation and post-separation behaviour is sensitive to the structure of the boundary layer as it approaches separation and, arising from this, also to structural features in the separated shear layer itself. The boundary layer is, in turn, materially influenced by the near-wall treatment, especially in the hill-crest region where y^+ values along the wall-nearest grid-line are high.

Fig. 1 demonstrates, by way of pressure contours, that the shear layer contains a coherent motion associated with the Kelvin–Helmholz-like vortices, a process identified most clearly in animations performed for this flow. This organised motion contributes directly to the turbulence level in the shear layer, as well as interacting sensitively with the temporal variation of the separation process. The details of the coherent component are, however, influenced by the near-wall treatment, and this link is thus one potential source for the variability in the statistical behaviour observed in Fig. 12.

Fig. 13 conveys the fact that the exceptional behaviour of the WW wall law displayed in Fig. 12 is not essentially due to the different velocity profile forming the basis of that wall law, but arises, primarily, from the nature of its implementation. The figure compares four solutions, two obtained with the point-wise and two with the cell-integrated implementations of the wall laws LL2 and WW. As seen, there is fairly close correspondence between the two point-wise forms (LL2 and WW-p) and similarly close agreement between the two cell-integrated variants. The latter pair both give solutions which are significantly closer to the highly-resolved simulation. This level of sensitivity to the

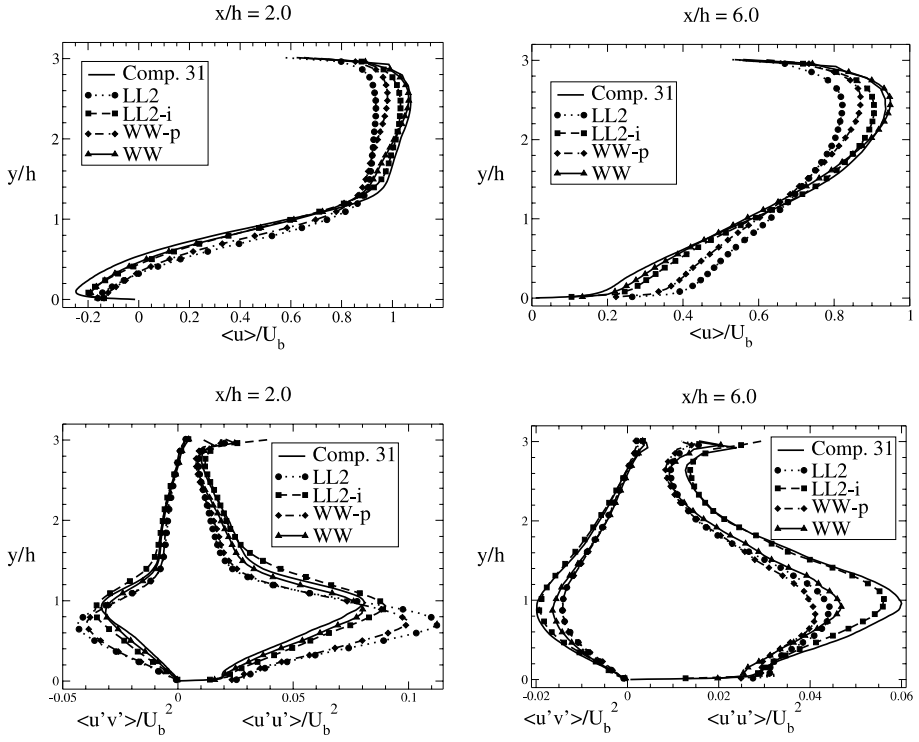

Fig. 13. Streamwise velocity, resolved streamwise stress and resolved shear stress at $x/h = 2$ and 6 using the point-wise and cell-integrated forms of LL2 and WW wall-treatments and the WALE model on the coarsest grid.

implementation details is remarkable, and is most likely linked to influential differences in the level of the wall-shear stress returned by the two implementations. A priori studies on plane, fully-developed channel flow, in which DNS velocity profiles were fed into both implementations of the LL2 and WW wall-functions, have shown that both integrated forms give consistently higher wall-shear values than the point-wise forms, the latter returning values that are closer to the DNS level when the wall-nearest node is beyond $y^+ = 16$. A higher wall-shear stress level (traction) just upstream of the separation point encourages, all other conditions being unchanged, a slightly earlier separation, apart from possibly influencing the organised behaviour in the shear layer, via the mechanism considered earlier.

The overall conclusions emerging from the above results is, therefore, that even relatively minor variations in the near-wall treatment can have major effects on the separation behaviour and the structural features in the separated layer, thus materially affecting gross flow features if the streamwise resolution is coarse, especially around the separation point.

8.4. Sensitivity to SGS models on the coarsest grid

An overall view of the sensitivity of the solution to SGS modelling, on the coarsest grid, is conveyed in Table 3, cases 8–12 and 2. In general, the coarser the grid, the more influential the SGS model is expected to be. Hence, it is of interest to undertake a study of the sensitivity to SGS modelling on Grid 1, even if this grid is known to offer relatively poor resolution in the separation region. All simulations were performed with the default (cell-integrated) form of the Werner–Wengle wall law (WW), shown earlier to give, alongside LL2-i, the most favourable agreement with the highly-resolved simulation.

Reference to Table 3 and to Figs. 14 and 15, the latter showing mean-velocity and turbulent-stress profiles, allows the overall observation that sensitivity to SGS modelling, even on the coarsest grid, is not especially pronounced, and this reinforces the comments made earlier about the importance of the near-wall approximation as the major source of variability among simulations on the coarsest grid.

The separation point is seen to be rather insensitive to the SGS model, while the reattachment point is somewhat more sensitive. This is a consequence of the dependence of the former primarily on the upstream near-wall flow, while the latter responds to both the separation point and the processes in the post-separation shear layer which are likely to be sensitive, to a greater extent, to SGS modelling. Among the SGS models, the WALE model and the MSM give the longest recirculation length, closest to the reference. The dynamic models, on the other hand, tend to return the shortest recirculation regions.

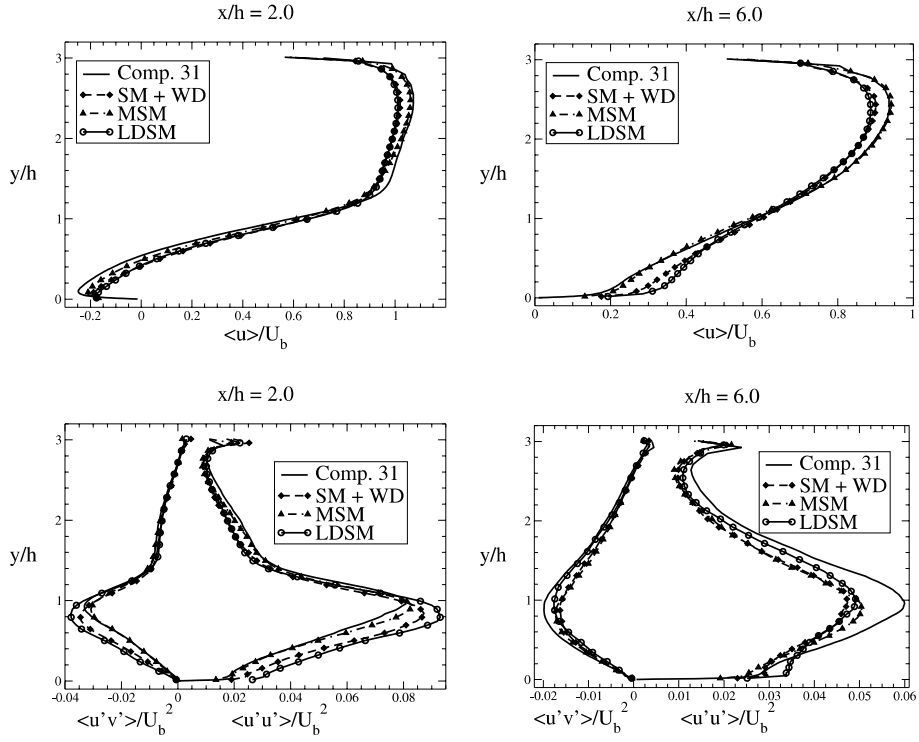

Fig. 14. Streamwise velocity, resolved streamwise stress and resolved shear stress at $x/h = 2$ and 6 using three SGS models together with the WW wall function on the coarsest grid.

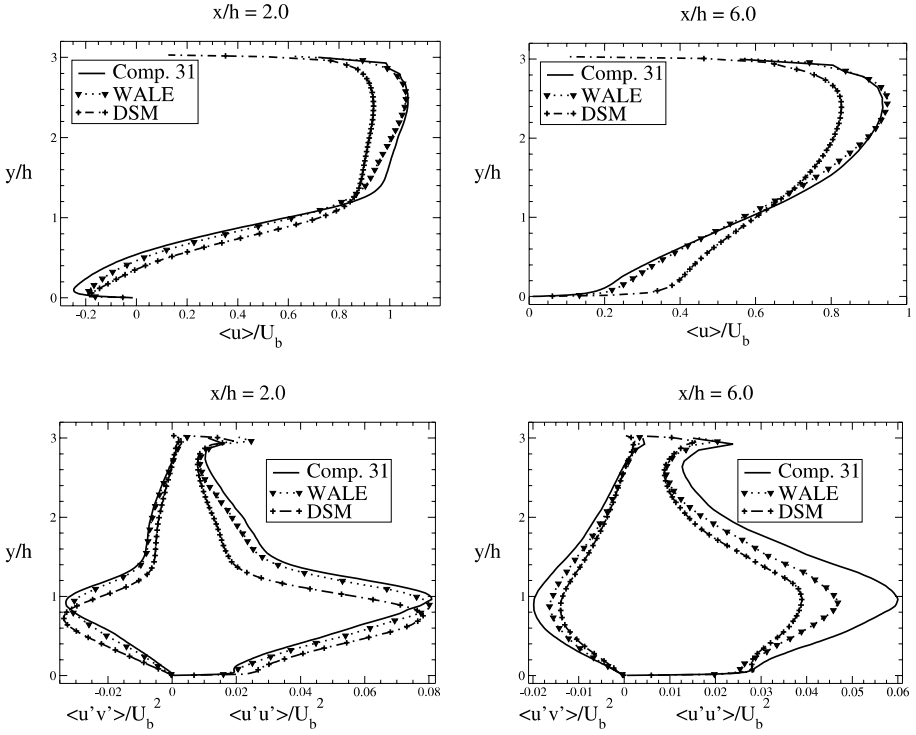

Fig. 15. Streamwise velocity, resolved streamwise stress and resolved shear stress at $x/h = 2$ and 6 using the WALE and the DSM model together with the WW wall function on the coarsest grid (computed with two different codes).

Since the SGS model affects the simulated solution via the introduction of an SGS viscosity, and hence SGS stresses, it is instructive to examine the level of viscosity returned by different models. To this end, profiles of the time-averaged SGS viscosity at the locations $x/h = 2$ and 6 are given in Fig. 16. As seen, the SGS viscosity level varies between approximately 1 and 4 times the fluid viscosity, with the mixed-scale and damped Smagorinsky models giving low values, the dynamic models giving high levels and the WALE model being in the middle of the range. While Table 3 suggests an association between low levels of SGS viscosity and long recirculation zones, and hence improved agreement with the reference simulation, this association is not unambiguous, as is exemplified by the result with the damped Smagorinsky model. Broadly consistent with the above trend is the observation, from Figs. 14 and 15, that models returning relatively low values of SGS viscosity (MSM, WALE, SM + WD) also give rise to lower values of resolved turbulent stresses and closer agreement with the reference simulation.

This is not a behaviour that concurs with initial expectations: a high SGS viscosity is expected to cause smoothing (damping) of the resolved scales close to the wave-number cut-off, and thus to lead to a reduction in the resolved stresses. The opposite would then be expected to occur when the SGS viscosity decreases. However, this line of reasoning is based on a consideration of isotropic turbulence, with the cut-off located well within the inertial range, not far from the dissipative

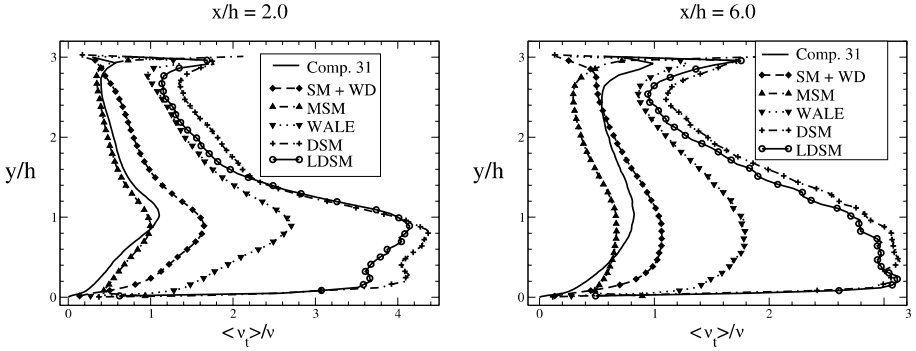

Fig. 16. SGS viscosity at $x/h = 2$ and 6 using five SGS models and the WW wall function on the coarsest grid.

limit. The present flow, in contrast, exhibits significant anisotropy in the resolved motion at the cut-off, due to the coarseness of Grid 1, and hence different energy-transfer characteristics across the large-scale part of the spectrum. This applies, in particular, to the post-separation shear layer. As noted earlier, by reference to Fig. 1, the shear layer contains anisotropic coherent structures with relatively large spanwise extent. Animations reveal that the vortices undergo fairly pronounced helical pairing, whilst breaking up as they are convected downstream. Higher viscosity slows down this process, tending to reduce the generation of spanwise fluctuation by a dynamic redistribution of kinetic energy. This encourages the persistence of the large-scale two-dimensional anisotropic features, which then tends to result in elevated levels of resolved fluctuations, as is observed in other configurations (Mellen et al., 2002a).

8.5. Comparisons for the medium Grid 2

In accord with expectation, refinement of the grid results in an improvement in the predicted flow, both in respect of the separation and the reattachment positions. At the same time, the dependence on the near-wall approximation declines, as is seen from Fig. 17. It is recalled, however, that the refinement is highly localised and selective, involving mainly an increase in the streamwise grid density in the vicinity of the hill crest. The result is a more accurate resolution of the separation process. The importance of this specific aspect of the simulation has been highlighted already by reference to the coarse-grid results. Evidently, it is this improvement which is principally responsible for the substantial overall improvement in the predicted flow field. Thus, the streamwise resolution, especially around the separation location, is clearly as influential as the near-wall approximation, if not more so. Reference to Fig. 17 shows that, among the wall treatments, the NS condition remains poor, while the Werner–Wengle approximation performs best, as it did with the coarse grid. In fact, the departure of the WW solution from the highly-resolved simulation is almost insignificant in respect of both the mean flow and turbulence quantitities. This simulation, case 24 in Table 3, also gives separation and reattachment points close to those of the highly-resolved solution.

The performance of the backflow model, Section 4.4, is contrasted in Figs. 18 and 19 to that returned by the Werner–Wengle approximation, the latter figure showing the predicted shear-stress distributions on the lower wall. Since the Werner–Wengle law yields a reasonably good representation of the highly-resolved variation, there is not much room for improvement when the backflow model is used on the same grid. Thus, the solution is similarly close to the reference solution. Also, the computed wall-shear stress is close to the reference variation over most of the backflow region. The small kink at the reattachment point is due to an implemen-

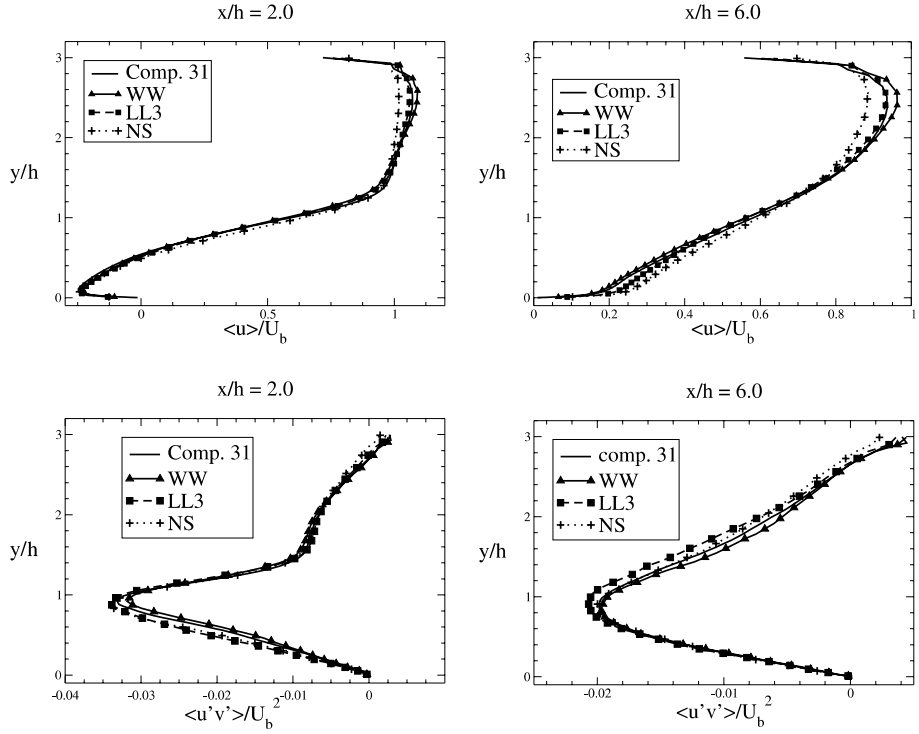

Fig. 17. Streamwise velocity and resolved shear stress at $x/h = 2$ and 6 using three near-wall approximations together with the WALE model on Grid 2.

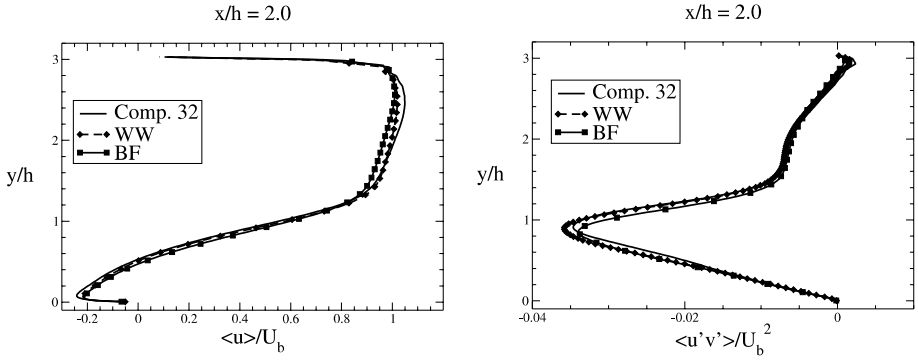

Fig. 18. Streamwise velocity and resolved shear stress at $x/h = 2$ using the WW and BF near-wall approximations together with the DSM model on Grid 2.

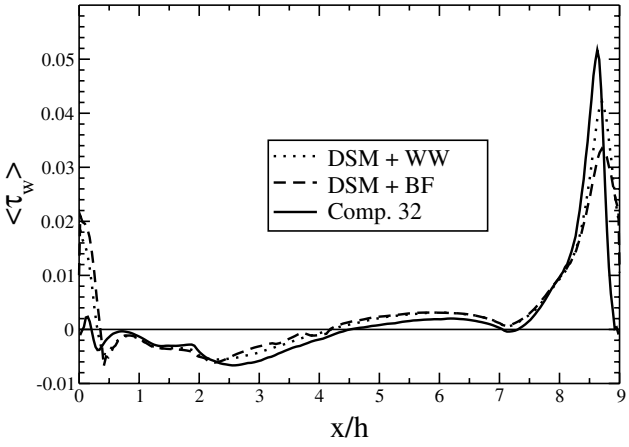

Fig. 19. Time-mean wall shear stress at the lower wall obtained with the SGS model in conjunction with the WW wall function, and with the DSM SGS model in conjunction with the BF wall function on Grid 2.

tational issue. When the recirculation bubble is thin, the maximum backflow velocity and its location fall into the first cell. This could be smoothed out by a slight adjustment of the formulation, but the local shear stress is so low as to render it uninfluential. To take greater advantage of the backflow model, the grid would have to be coarser near the wall. With the current grid, the distance of the wall-adjacent grid point in the recirculation zone, in wall units, reaches a maximum of approximately 5 at around $x/h = 2$ and is smaller elsewhere in the bubble (Fig. 11). For a higher Reynolds number, the difference between the WW and the backflow model would be expected to be larger.

The sensitivity to SGS modelling on the medium grid is shown in Figs. 20 and 21 for $x/h = 2$ only. Four solutions are included, corresponding to cases 24–27 in Table 3, all obtained with the WW wall approximation. The WALE, SM, and DSM SGS models all return broadly satisfactory solutions. WALE and DSM perform slightly better than SM, but the overall variation is small.

An exception is the DMM, which performs less satisfactorily. The present implementation includes spanwise averaging to regularize the dynamic coefficient and no further smoothing. Unfortunately, point-to-point oscillations in the viscosity are created near the walls, and these cause an abnormal behaviour, especially at the upper wall where oscillations are most pronounced. The origin of the problem is probably the explicit grid filtering this model involves (see Section 3.3). When the DMM is used on a wall-resolving grid for low-*Re* channel flow, the results are good—indeed, even better

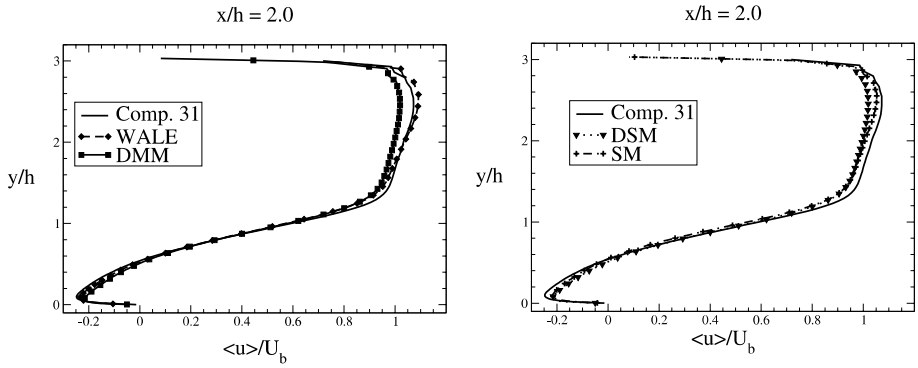

Fig. 20. Streamwise velocity at $x/h = 2$ using four SGS models together with the WW near-wall approximations on Grid 2.

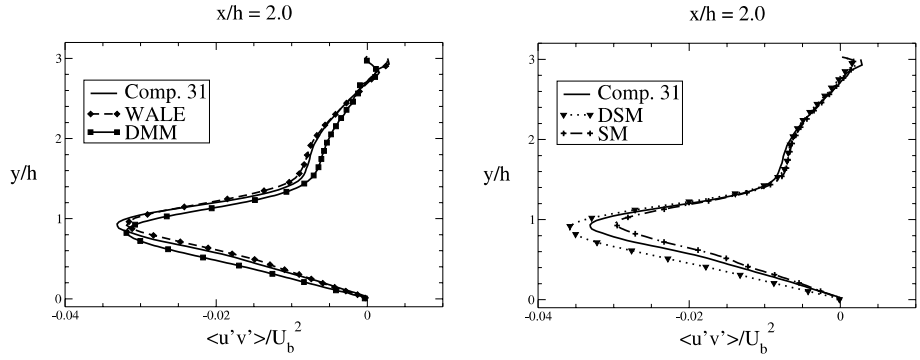

Fig. 21. Resolved shear stress at $x/h = 2$ using four SGS models together with the WW near-wall approximations on Grid 2.

than those returned by the DSM. Here, however, the wall-function grid is coarse, generating high gradients at the boundaries and large entries in the Leonard tensor and thus introducing too much backscatter which is not sufficiently damped by the eddy viscosity. This behaviour was not observed in the study by Salvetti et al. (2001), where a two-parameter model, similar to the present form, was applied within a coarse-grid simulation of a wavy-terrain flow. It is possible that the more successful application of the model in that study is associated with the NS and free-slip conditions applied at the lower wall and free upper boundary, respectively.

9. Conclusions

Large eddy simulations of a fully turbulent flow separating from a curved wall in a channel have been presented. The emphasis of the study has been on identifying the influence of resolution, SGS modelling and near-wall modelling on the accuracy of the simulations. Employing two different codes with the same grids allowed careful cross-checking to be done, thus enhancing confidence in the results.

Simulations on a coarse grid have highlighted the outstanding importance of an adequate streamwise resolution of the flow in the vicinity of the separation line. This importance arises from the fact that the reattachment position is highly sensitive to that of separation, and so is the entire flow. Although the separation line varies in time over a substantial region around the mean location, the precision with which the latter is predicted is, at best, of the order of the local mesh size. In specific terms, a streamwise resolution of $0.08h$ around the mean separation location can be expected to produce an error margin in the reattachment position of order $0.5h$. Indeed, the present study suggests that this is a rather optimistic estimate.

The dependence of the solution on different practices of near-wall and SGS modelling has been investigated on two grids and compared to highly-resolved reference simulations. The results have been found to be surprisingly sensitive to the nature of the numerical implementation of the wall laws, rather than to the precise assumptions of the velocity profiles underpinning them. The best performance was obtained with cell-integrated implementations of either the log-law or the Werner–Wengle approximation. The differences between the point-wise and cell-integrated implementations is due to the latter returning higher levels of wall-shear stress than the former, all other conditions being the same. This encourages earlier separation and hence better correspondence with the highly resolved simulation. The BF wall law, while resting on a firmer physical foundation in the presence of recirculation, was not found to offer clear predictive advantages in the flow investigated herein.

It must be acknowledged that the relatively low Reynolds-number of the flow led to the wall-nearest computational point lying within the semi-viscous wall layer over most of the lower wall bordering the separation zone. Also, a priori studies, exploiting the highly-resolved simulation data, have demonstrated that the near-wall flow did not conform to the velocity profiles underpinning the wall laws, except for the case of backflow wall law within the recirculation zone. This inevitably limits the generality of the conclusions derived in respect of near-wall modelling.

The sensitivity of the solution to SGS modelling has been found to be weaker than to variations in resolution and near-wall treatment. Of the SGS models examined, the WALE and the MSM performed best, in so far as the related coarse-grid solutions came closest to the highly-resolved simulation. Both models returned relatively low levels of SGS viscosity, although the latter was shown to give an incorrect wall-asymptotic viscosity variation in wall-resolved channel-flow simulations.

Further studies are clearly needed for flows at higher Reynolds numbers, but this poses the problem of generating sufficiently detailed and accurate benchmark data at tolerable cost. The present study at least suggests that resolution parameters are likely to be especially

critical in other flows involving separation from gently curved surfaces, such as highly-loaded aerofoils and blades. Configurations of this type arguably require preferential attention to identify the capabilities of LES in conditions more challenging than those examined herein. Particularly interesting would also be the application of an unstructured LES method, capable of local refinement near the crest of the hill, including refinement in the spanwise direction.

Acknowledgements

The authors gratefully acknowledge helpful and stimulating discussions with W. Rodi. Temmerman and Mellen acknowledge the financial support provided by the European Commission through the Framework V BRITE/EURAM project 'LESFOIL'. Fröhlich has been funded through the DFG-CNRS research initiative 'Numerical Flow Simulation'. The simulations undertaken by Temmerman and Leschziner were made possible by the provision of computer resources on the CSAR Cray T3E national facility in Manchester, through a grant from the UK Engineering and Physical Sciences Research Council. Those by Mellen and Fröhlich could be performed thanks to the provision of resources on the IBM-SP computer of the Karlsruhe Computer Center.

References

Almeida, G.P., Durão, D.F.G., Heitor, M.V., 1993. Wake flows behind two-dimensional model hills. Experim. Therm. Fluid Sci. 7, 87–101.

Armenio, V., Piomelli, U., 2000. A Lagrangian mixed subgrid-scale model in generalized coordinates. Flow, Turb. Combust. 65 (1), 51–81.

Balaras, E., Benocci, C., Piomelli, U., 1996. Two-layer approximate boundary conditions for large-eddy simulations. AIAA J. 34 (6), 1111–1119.

Bardina, J., Ferziger, J.H., Reynolds, W., 1980. Improved subgrid-scale models for large–eddy simulation. AIAA—Paper no. 80-1357.

Breuer, M., Rodi, W., 1994. Large eddy simulation of turbulent flow through a straight square duct and a 180° bend. In: Voke, P.R., Kleiser, R., Chollet, J.P. (Eds.), Fluid Mech. and its Appl., vol. 26. Kluwer Academic, pp. 273–285.

Breuer, M., Rodi, W., 1996. Large eddy simulation of complex turbulent flows of practical interest. In: Hirschel, E.H. (Ed.), Flow Simulation with High Performance Computers II, vol. 52 of Notes on Numerical Fluid Mechanics. Vieweg, Braunschweig, pp. 258–274.

Cabot, W., Moin, P., 1999. Approximate wall boundary conditions in the large eddy simulation of high Reynolds number flow. Flow, Turbul. Combust. 63, 269–291.

Davidson, L., September 2000. LESFOIL: A European project on large eddy simulations around a high-lift airfoil at high Reynolds number. In: ECCOMAS 2000, European Congress on Computational Methods in Applied Sciences and Engineering, Barcelona, Spain.

Davidson, L., Peng, S.-H., 2001. A hybrid LES-RANS model based on a one-equation SGS model and a two-equation k–ω model. In: Lindborg, E., Johansson, A., Eaton, J., Humphrey, J., Kasagi, N., Leschziner, M., Sommerfeld, M. (Eds.), Turbulence and Shear Flow Phenomena. Second International Symposium. Stockholm, KTH, pp. 175–180.

Deardorff, J.W., 1970. A numerical study of three-dimensional turbulent channel flow at large Reynolds numbers. J. Fluid Mech. 41, 453–480.

Devenport, W.J., Sutton, E.P., 1991. Near-wall behavior of separated and reattaching flows. AIAA J. 29 (1), 25–31.

di Mare, F., Jones, W.P., 1999. Large eddy simulation of the vortex shedding process in the near-field wake behind a square cylinder. In: Allan, R.J., Guest, M.F., Simpson, A.D., Henty, D.S., Nicole, A.D. (Eds.), High-Performance Computing. Kluwer Academic/Plenum Publishers, pp. 439–450.

Ducros, F., Nicoud, F., Poinsot, T., 1998. Wall-adapting local eddy-viscosity models for simulations in complex geometries. In: 6th ICFD Conference on Numerical Methods for Fluid Dynamic. pp. 293–299.

Germano, M., 1998. Fundamentals of large eddy simulations. In: Advanced Turbulent Flow Computations. Springer-Verlag, pp. 1760–1765.

Germano, M., Piomelli, U., Moin, P., Cabot, W.H., 1991. A dynamic subgrid-scale eddy viscosity model. Phys. Fluids A 3 (7), 1760–1765.

Grötzbach, G., 1987. Direct numerical and large eddy simulation of turbulent channel flows. Encyclopedia Fluid Mech. 6, 1337–1391.

Henn, D.S., Sykes, R.I., 1999. Large-eddy simulation of flow over wavy surfaces. J. Fluid Mech. 383, 75–112.

Hinze, J., 1975. Turbulence. McGraw-Hill.

Hoffmann, G., Benocci, C., 1994. Simulation of spatially-developing planar jets. In: 74th Fluid Dynamics Symposium on "Applications of Direct and 32 Large Eddy Simulation", Chania, Crete, Greece. pp. 261–266.

Jansen, K., 1996. Large-eddy simulations of flow around a NACA 4412 airfoil using unstructured grids. In: Annual Research Briefs (CTR). pp. 225–232.

Jiménez, J., Moin, P., 1991. The minimal flow unit in near-wall turbulence. J. Fluid Mech. 225, 213–240.

Jones, W.P., Wille, M., 1996a. Large eddy simulation of a round jet in a cross-flow. In: Engineering Turbulence Modelling III. pp. 439–450.

Jones, W.P., Wille, M., 1996b. Large eddy simulation of a plane jet in a crossow. Int. J. Heat Fluid Flow 17 (3), 296–306.

Kaltenbach, H.J., Choi, H., 1995. Large-eddy simulations of flow around an airfoil on a structured mesh. In: Annual Research Briefs (CTR). pp. 51–60.

Kaltenbach, H.J., Fatica, M., Mittal, R., Lund, T.S., Moin, P., 1999. Study of flow in a planar asymmetric diffuser using large-eddy simulation. J. Fluid Mech. 390, 151–185.

Lardat, R., Leschziner, M., 1998. A Navier–Stokes solver for LES on parallel computers. Tech. Rep., Department of Mech. Eng., UMIST.

Launder, B.E., Spalding, D.B., 1974. The numerical computation of turbulent flows. Comp. Meth. Appl. Mech. Engrg. 3, 269–289.

Le, H., Moin, P., Kim, J., 1997. Direct numerical simulation of turbulent flow over a backward-facing step. J. Fluid Mech. 330, 349–374.

Lesieur, M., Métais, O., 1996. New trends in large eddy simulations. Ann. Rev. Fluid Mech. 28, 45–82.

Lilly, D.K., 1992. A proposed modification of the Germano subgrid-scale closure method. Phys. Fluids A 4 (3), 633–635.

Mathey, F., Fröhlich, J., Rodi, W., 1999. LES of heat transfer in turbulent flow over a wall mounted matrix of cubes. In: Voke, P., Sandham, N., Kleiser, L. (Eds.), Direct and Large-Eddy Simulation III. Kluwer Academic, pp. 51–62.

Mathey, F., Fröhlich, J., Rodi, W., On the scaling in recirculating flows and its use as a wall model for large eddy simulation, in preparation.

Meinke, M., Krause, E., 1998. Applications of LES to jets and internal turbulent flows. In: Advanced Turbulent Flow Computations. Springer-Verlag, pp. 155–208.

Mellen, C.P., Fröhlich, J., Rodi, W., 2000. Large eddy simulation of the flow over a periodic hill. In: 16th IMACS World Congress 2000, Lausanne.

Mellen, C.P., Fröhlich, J., Rodi, W., 2002a. Lessons from the european LES-FOIL project on LES of flow around an airfoi. AIAA—Paper no. 2002-0111.

Mellen, C.P., Fröhlich, J., Rodi, W., Temmerman, L., Leschziner, M.A., 2002b. Highly-resolved large eddy simulation of separated flow in a streamwise periodic channel constriction, in preparation.

Moin, P., 1998. Numerical and physical issues in large eddy simulation of turbulent flows. JSME Int. J., Ser. B 41 (2), 454–463.

Moser, R.D., Kim, J., Mansour, N.N., 1999. Direct numerical simulation of turbulent channel flow up to $Re_\tau = 590$. Phys. Fluids 11 (4), 943–945.

Murakami, S., Rodi, W., Mochida, A., Sakamoto, S., 1993. Large eddy simulation of turbulent vortex shedding flow past 2d square cylinders. In: Engineering Applications of Large Eddy Simulations 1993, ASME FED Publication 162, pp. 113–120.

Nikitin, N.V., Nicoud, F., Wasisto, B., Squires, K.D., Spalart, P.R., 2000. An approach to wall modelling in large–eddy simulations. Phys. Fluids 12 (7), 1629–1632.

Piomelli, U., Liu, J., 1995. Large-eddy simulation of rotating channel flows using a localized dynamic model. Phys. Fluids 7 (4), 839–848.

Rhie, C.M., Chow, W.L., 1983. Numerical study of the turbulent flow past an airfoil with trailing edge separation. AIAA J. 21 (11), 1525–1532.

Rodi, W., 1998. Large-eddy simulations of the flow past bluff bodies: state-of-the art. JSME Int. J., Ser. B 41 (2), 361–373.

Sagaut, P., 1996. Simulations of separated flows with subgrid models. La Recherche Aérospatiale 1, 51–63.

Salvetti, M.V., Damiani, R., Beux, F., 2001. Three-dimensional coarse large-eddy simulations of the flow above two-dimensional sinusoidal waves. Int. J. Numer. Meth. Fluids 35 (6), 617–642.

Schumann, U., 1975. Subgrid scale models for finite difference simulations of turbulent flows in plane channels and annuli. J. Comp. Phys. 18, 376–404.

Schumann, U., Sweet, R.A., 1988. Fast Fourier transforms for direct solution of Poisson's equation with staggered boundary conditions. J. Comp. Phys. 75, 123–137.

Shur, M., Spalart, P.R., Strelets, M., Travin, A., 1999. Detached-eddy simulation of an airfoil at high angle of attack. In: Rodi, W., Laurence, D. (Eds.), Engineering Turbulence Modelling and Experiments—4, Ajaccio, France. Elsevier, pp. 669–678.

Simpson, R.L., 1983. A model for the backflow mean velocity profile. AIAA J. 21 (1), 142–143.

Smagorinsky, J., 1963. General circulation experiments with the primitive equations, I, the basic experiment. Mon. Weather Rev. 91, 99–165.

Spalart, P.R., Jou, W.-H., Strelets, M., Allmaras, S.R., 1997. Comments on the feasibility of LES for wings and on the hybrid RANS/LES approach. In: Advances in DNS/LES, 1st AFOSR International Conference on DNS/LES. Greyden Press, pp. 137–148.

Stone, H.L., 1968. Iterative solution of implicit approximations of multidimensional partial differential equations for finite difference methods. SIAM J. Numer. Anal. 5, 530–558.

Temmerman, L., Leschziner, M., Ashworth, M., Emerson, D., 2000. LES applications on parallel systems. In: Jenssen, C.B. (Ed.), Parallel Computational Fluid Dynamics 2000, Trondheim, Norway. Elsevier, pp. 465–474.

Thomas, T.G., Williams, J.J.R., 1999. Large eddy simulation of vortex shedding from cubic obstacle. J. Aerospace Eng. 113, 113–121.

Van Driest, E.R., 1956. On the turbulent flow near a wall. J. Aero. Sc. 23, 1007–1011.

Werner, H., Wengle, H., 1991. Large-eddy simulation of turbulent flow over and around a cube in a plate channel. In: 8th Symposium on Turbulent Shear Flows. pp. 155–168.

Wille, M., 1997. Large eddy simulation of jets in cross flows. Ph.D. thesis, Imperial College of Science, Technology and Medicine,University of London, London, UK.

Zang, Y., Street, R.L., Koseff, J.R., 1993. A dynamic mixed subgrid-scale model and its application to turbulent recirculating flows. Phys. Fluids A 5 (12), 3186–3196.